# 15

# Tunable mid-infrared laser absorption spectroscopy

F. K. TITTEL and R. LEWICKI, Rice University, USA

**DOI**: 10.1533/9780857096401.3.579

**Abstract**: This chapter discusses state-of-the-art spectroscopic techniques based on mid-infrared laser absorption spectroscopy (LAS) and recent examples of their use in field deployable optical instruments for real-world applications. Optimum mid-infrared LAS performance depends on three interrelated technologies: spectroscopic detection method, laser source and a detector matched to the detection technique and laser source. Hence a critical component of LAS is the use of various well established and novel detection methods that include several types of multipass gas absorption cells with the option to apply wavelength, frequency and amplitude modulation to the laser source. In addition various other instrumentation configurations based on cavity-enhanced spectroscopy (CES) have been developed to increase the magnitude of a molecular trace gas absorption signal. Other extremely useful mid-infrared detection schemes are direct open path monitoring (with and without retro-reflector) or indirect techniques based on photoacoustic and photothermal phenomena.

A significant improvement to trace gas detection systems using LAS methods has been achieved with the development of high performance semiconductor lasers, in particular tunable quantum cascade lasers (QCLs), since 1994. This has led to increased spectral resolution and high detection sensitivity of molecular trace gas species in the mid-infrared. Trace gas optical spectroscopic sensors based on QCLs are capable of real time, ultra-sensitive detection of trace gas molecular species that vary from the per cent level down to parts per trillion (ppt). Such sensors can be used in a wide range of applications that include environmental monitoring, medical and biomedical diagnostics, public health issues, industrial process control and analysis as well as national defense and security. In this chapter the spectroscopic detection and monitoring of various specific molecular species – such as $NH_3$, NO and $NO_2$ – is described based on cavity ring-down spectroscopy (CES), conventional and quartz-enhanced photoacoustic spectroscopy (CPAS and QEPAS) as well as Faraday rotation spectroscopy (FRS).

**Key words**: laser absorption spectroscopy, cavity enhanced spectroscopy, photoacoustic and quartz-enhanced spectroscopy, Faraday rotation spectroscopy, quantum and interband cascade lasers, environmental monitoring, breath analysis.

## 15.1 Introduction

Laser-based spectroscopic techniques are useful for the quantitative detection and monitoring of molecular trace gas species in the mid-infrared spectral region. The spectroscopic instrumentation generates a measurable signal that depends on the absorption of the target medium. The choice of an optimum detection scheme depends on the requirements of the specific application and the characteristic features of the infrared laser source. Well established detection methods include several types of multipass gas absorption cells with the option to apply wavelength, frequency and amplitude modulation to the laser source. Intra and external cavity-enhanced spectroscopy are two methods to increase the magnitude of the absorption signal. Photoacoustic and photothermal, open path monitoring (with and without retro-reflector), such as light detection and ranging (LIDAR), differential optical absorption spectroscopy (DOAS) laser induced fluorescence (LIF), laser breakdown spectroscopy (LIBS) and fiberoptic or waveguide evanescent wave spectroscopy are other useful mid-infrared detection schemes. A key optical component for LAS has been the introduction and commercial availability of high performance semiconductor lasers, in particular quantum cascade lasers (QCLs) since 1994 (Faist *et al.*, 1994) and interband cascade lasers since 1995–96 (Yang, 1995; Meyer *et al.*, 1996). The development of both QCLs and ICLs continues worldwide (Capasso, 2010; Vurgaftman *et al.*, 2010; Razeghi *et al.*, 2010; Bismuto *et al.*, 2011; Gupta *et al.*, 2010; Zeller, 2010). QCLs are convenient mid-infrared sources for ultra sensitive and highly selective trace gas monitoring as the result of recent advances in their design and technology. They can be fabricated to operate over a wide range of mid-infrared wavelengths from ~3 to ~24 μm. Continuous wave (CW) QCL devices capable of thermo-electrically cooled, room-temperature operation with several important practical features – including single mode emission with mode-hop free frequency tuning, high power (tens to hundreds of mWs), and intrinsic narrow emission line widths – are commercially available in the ~4–12 μm spectral region (Curl *et al.*, 2010; Capasso *et al.*, 2010). These spectral characteristics permit the development of robust and fieldable trace gas sensors (Kosterev and Tittel, 2002; McManus *et al.*, 2010; Lee *et al.*, 2011; Lewicki *et al.*, 2011). For example, the Rice Laser Science group has explored the use of several methods for carrying out infrared laser absorption spectroscopy (LAS) with mid-infrared QCL and interband cascade laser (ICL) sources, which include multipass absorption spectroscopy (Weidmann *et al.*, 2005), cavity ring down spectroscopy (CRDS) (Kosterev *et al.*, 2001), integrated cavity output spectroscopy (ICOS) (Bakhirkin *et al.*, 2006; McCurdy *et al.*, 2007b), photoacoustic spectroscopy (PAS) and quartz-enhanced photoacoustic spectroscopy (QEPAS) (Kosterev *et al.*,

2005a; Lewicki *et al*, 2007b; Dong *et al*, 2010; Kosterev *et al*, 2010b), as well as Faraday rotation spectroscopy (Lewicki *et al.*, 2009; Zaugg *et al.*, 2011). These spectroscopic techniques permit the detection and quantification of molecular trace gases with demonstrated detection sensitivities ranging from ppmv to pptv levels depending on the specific gas species and the detection method employed.

## 15.2 Laser absorption spectroscopic techniques

In conventional absorption spectroscopy (CAS), using broadband incoherent radiation sources, such as thermal emitters, the wavelength resolution is determined by the resolving power of the spectral analyzer or spectrometer. LAS, on the other hand, uses coherent light sources, whose linewidths can be ultra-narrow and whose spectral densities can be made many orders of magnitude larger (~$10^9$W/(cm$^2$MHz)) than those of incoherent light sources. The key advantages of mid-infrared LAS include the following.

1. An absorption spectrum that can be acquired directly by scanning the laser source across a desired rotational-vibrational resolved feature of the target analyte.
2. High detection sensitivity with maximum accuracy and precision.
3. Improved spectral selectivity or resolution compared with CAS due to the narrow linewidths (i.e. for CW QCLs ~0.1–3 MHz with a high quality power supply or <10 kHz with frequency stabilization and for pulsed QCLs ~300 MHz).
4. Fast response time.
5. Good spatial resolution. This can involve remote sensing via LIDAR, a mobile laboratory, aircraft, or networks of ground- or marine-based sensors.
6. Detector noise that becomes negligible for sufficiently large laser intensities.
7. Non-intrusive methods, such as balanced detection or zero air subtraction, to suppress laser intensity fluctuations that can be readily applied to increase the signal-to-noise ratio (SNR) and hence improve the LAS detection sensitivity, i.e. the minimum detectable absorption limit.
8. Spatially coherent laser light that can be collimated, which allows the use of long pathlength absorption and cavity-enhanced spectroscopy (CES) cells.
9. The laser frequency can be locked to the center of a resolved molecular absorption line to determine the center wavelength or wavenumber of the line with ultra-high precision and accuracy.

10. Size, weight, electrical power, thermal management, gas and wavelength calibration, protection from harsh environment, autonomous operation and remote access for long periods of time.
11. Ease of instrument operation and data reduction.

### 15.2.1 Laser absorption spectroscopy

During the past 25 years, mid-infrared LAS techniques have become extremely sensitive, commercially available and effective spectroscopic tools from ~ 3 to 12 μm (it should be noted that Sb-based laser diodes, ICLs and QCLs spectral coverage from 2 to 24 μm has been demonstrated and reported in the literature (Belenky *et al.*, 2011; Christensen *et al.*, 2010; Curl *et al.*, 2010; Capasso, 2010) for the detection and quantification of numerous molecular trace gas species. As result of these LAS advances, molecular trace gases can now be measured in ultra small quantities in numerous laboratory and field applications. Furthermore, single atoms and different isotopes of the same atom can be detected for different chemical species. In the mid-infrared region, the optical sensor systems, which employ different spectroscopic techniques, can be employed to obtain detection sensitivities in the parts per million by volume (ppmv) to parts per trillion by volume (pptv) range, depending on the specific gas species and the detection method employed. These high sensitivities are obtained using various overtone combination and fundamental rotational-vibrational molecular absorption bands located between the 3 and 24 μm wavelengths of the mid-infrared region. The mid-infrared absorption spectra of several small molecules of potential interest for trace gas monitoring are shown in Fig. 15.1 within two mid-infrared atmospheric transmission windows.

The primary requirements for trace gas sensing are sensitivity and selectivity. For small molecules with resolved rotational structure, the selectivity is obtained by choosing an absorption line that is free of interference from other species that might be present in the analyzed sample. Moreover, selectivity is obtained by implementing a laser source that possesses a sufficiently narrow linewidth. For small molecules, reducing the sample pressure sharpens the absorption line without reducing the peak absorption, which significantly improves selectivity. This condition continues until the linewidth begins to approach the Doppler width (Kosterev *et al.*, 2008).

Fundamentals of the LAS at a certain frequency $\upsilon$ ($cm^{-1}$) can be expressed by Beer–Lambert's law:

$$I(\upsilon) = I_o(\upsilon)e^{-\alpha(\upsilon)L} \qquad [15.1]$$

where $I(\upsilon), I_o(\upsilon)$ are the intensity of transmitted and incident laser light, $\alpha(\upsilon)$ is the absorption coefficient ($cm^{-1}$), and $L$ is the effective optical

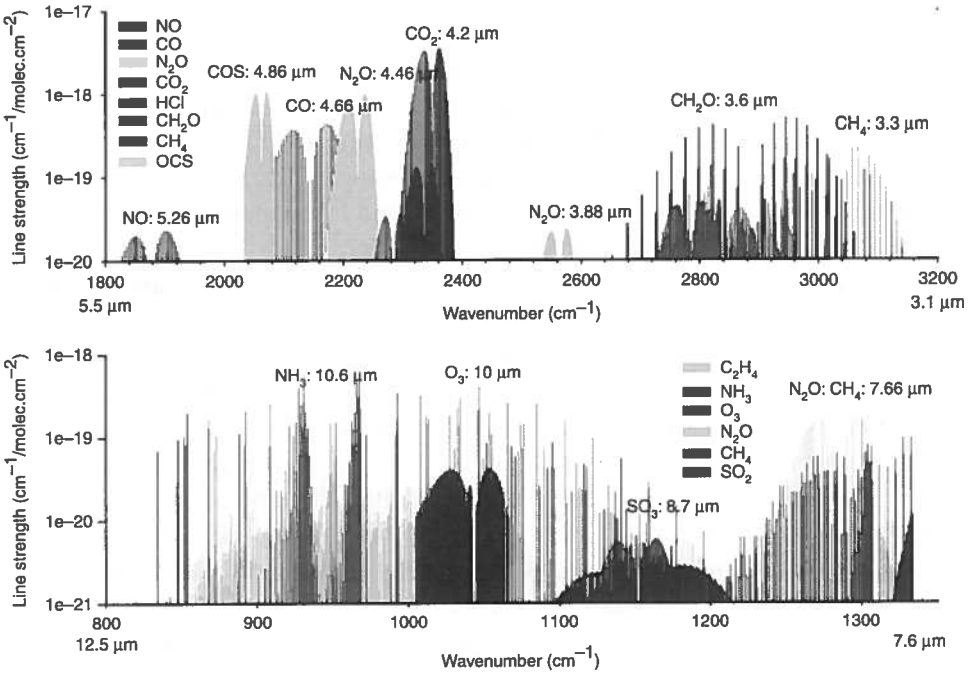


*15.1* High-resolution transmission molecular absorption database (HITRAN) simulation of absorption spectra in two mid-infrared atmospheric transmission windows (Kosterev, 2008).

path-length (cm). Therefore, to obtain the best absorption sensitivity one needs to choose a strong molecular absorption line, use a long effective optical path-length, and have a distinguishable absorption from baseline variations and laser power fluctuations. The first requirement is best met by choosing a target line associated with fundamental absorption bands, as these are stronger than overtone or combination bands. A sufficiently long path-length can be obtained by using multipass cells or cavity enhancement techniques. For sharp absorption lines, noise associated with laser power fluctuations can be reduced by averaging rapid scans over the line or by employing the wavelength modulation spectroscopy (WMS) technique in the kHz regime (Schilt *et al.*, 2003; Schilt and Thévenaz, 2006). In most applications, one detects the modulated absorption at twice the modulation frequency using a lock-in amplifier set to 2f. The second harmonic signal is maximum at the absorption line center. The final requirement to distinguish absorption from baseline variations is the most challenging. Every long pass arrangement exhibits accidental etalons, which typically have widths comparable to that of an absorption line. In principle, these can be removed by evacuating the cell, replacing the sample with 'zero air' gas, which contains no trace gas species of interest, and then dividing the sample trace by this

background trace. However, this approach assumes that these accidental etalons do not shift their pattern during the process of sample replacement, although this is often not the case (Curl *et al.*, 2010). Numerous research groups (Fried *et al.*, 1997, 1998; Fried and Richter, 2007; Zahniser *et al.*, 1995; Werle *et al.*, 2011) have investigated and reported on the merits of rapid background subtraction in particular WMS and frequency modulation spectroscopy (FMS) to effectively remove optical noise.

For more complex, multi-atomic molecules, which do not have resolved rotational structure, the spectroscopic detection process is more demanding. The only way to detect absorption is through the process of pumping the sample out and replacing it with zero air, due to the absence of a nearby baseline for comparison. For weak absorption features, this imposes severe limits on the long-term power stability of the laser source, the absence of low frequency laser noise, and baseline stability. Furthermore, in the mid-infrared fingerprint region, where many gases absorb, there may be other gases contributing to a broad absorption that might significantly disrupt the selectivity of concentration measurements.

For open path systems, a serious risk for selective measurements might be encountered because (1) there is no way to replace the sample with zero air for providing a baseline trace, and (2) there is no way to reduce the linewidths (typically 0.1 $cm^{-1}$ at atmospheric pressure), which in some cases might be too large to perform wavelength modulation spectroscopy at an optimum modulation depth. Obtaining a long path-length by using a multipass cell suffers from neither of these problems. The only issue with this approach is that long path multipass cells are intrinsically bulky. Long optical pathlengths are obtained by employing multipass absorption cells where the optical beam is reflected back and forth between concave mirrors. Numerous implementations have been reported in the literature, but four fundamental designs (White, Herriott, astigmatic Herriott and Chernin) have been used to achieve optical pathlengths of ~ 100 m physical lengths for ~0.5 m distance between the mirrors (McManus *et al.*, 1995). Cavity ringdown spectroscopy (CRDS) has been demonstrated to give excellent sensitivity (Kosterev *et al.*, 2001; Tittel *et al.*, 2003; Rao and Karpf, 2010), but requires very high quality, low loss mirrors. Long path lengths in small volumes can be provided by off-axis integrated cavity output spectroscopy (ICOS) which has considerable promise for trace gas sensing (Bakhirkin *et al.*, 2004; Bakhirkin *et al.*, 2006; McCurdy *et al.*, 2007b). Other ultra-sensitive and highly selective spectroscopic techniques that are employed by research groups for trace gas detection are: balanced detection (Sonnenfroh *et al.*, 2001), laser induced breakdown spectroscopy (LIBS) (Gottfried *et al.*, 2009), noise immune cavity enhanced optical heterodyne molecular spectroscopy (NICE-OHMS) (Ye *et al.*, 1998; Foltynowicz *et al.*, 2008), conventional photoacoustic spectroscopy (CPAS) (Elia *et al.*, 2009; Lima *et al.*,

2006), quartz-enhanced photoacoustic spectroscopy (QEPAS) (Kosterev and Tittel 2004; Kosterev *et al.*, 2005b), and Faraday rotation spectroscopy (FIS) (Litfin *et al.*, 1980; Ganser *et al.*, 2003; Lewicki *et al.*, 2009). The latter three techniques, and CRDS and ICOS will be described in the following sections of this chapter.

### 15.2.2 Cavity enhanced spectroscopy: CRDS and ICOS

The conventional method to perform sensitive laser-based absorption spectroscopy measurements is to increase optical path-length by using an optical multipass gas cell. However, such an approach can be difficult to implement in certain field applications, requiring compact gas sensor configurations. For example, a typical commercial 100 m path-length multipass cell has a volume of 3.5 l (Curl, 2010). An alternative way to obtain a long optical path is to make the light bounce along the same path between two ultralow-loss dielectric mirrors forming a high finesse optical resonator, called a ringdown cavity (RDC) Cavity ring-down spectroscopy is based on the principle of measuring the rate of decay of light intensity inside the RDC. The transmitted wave from an injected pulsed or CW laser into the CRD decays exponentially in time. The decay rate is proportional to the losses inside the RDC. For typical RDC mirrors having a reflectivity of 99.995%, and spaced ~20 cm, an effective optical pathlength of 8 km is obtained, which exceeds the best performance of multi-pass cell spectroscopy. The light leaking out of the RDC can be used to characterize the absorption of the intracavity medium. The optical loss is the difference between total cavity losses and empty cavity losses. Once the absorption spectrum of the sample has been measured, then the sample concentration can be determined using the absorption cross-section and the lineshape parameters. A good CRDS system can achieve a minimum detectable absorption limit of $\sim 4 \times 10^{-10}$. Detailed mathematical treatment of CRDS can be found in the literature (Busch and Busch 1999; Paldus and Kachanov 2005).

Several techniques exist to perform CRDS (O'Keefe and Deacon 1988; Ramponi *et al.*, 1988; Scherer *et al.*, 1997) or integrated cavity output spectroscopy (ICOS) and its variant, off-axis ICOS (OA-ICOS), a technique where one observes time integrated ring-down events (O'Keefe, 1998; O'Keefe *et al.*, 1999; Bakhirkin *et al.*, 2004; McCurdy *et al.*, 2007b). In these techniques the coupling efficiency of the laser radiation into the resonant cavity is extremely critical and determines the amount of light which can be collected by a photodetector placed after the absorption cell.

The CRDS technique is intrinsically background-free. When carried out with high power pulsed lasers, CRDS requires only high quality cavity mirrors, a reasonably fast detector and appropriate data acquisition electronics. This technique is harder to implement with QCLs, which have

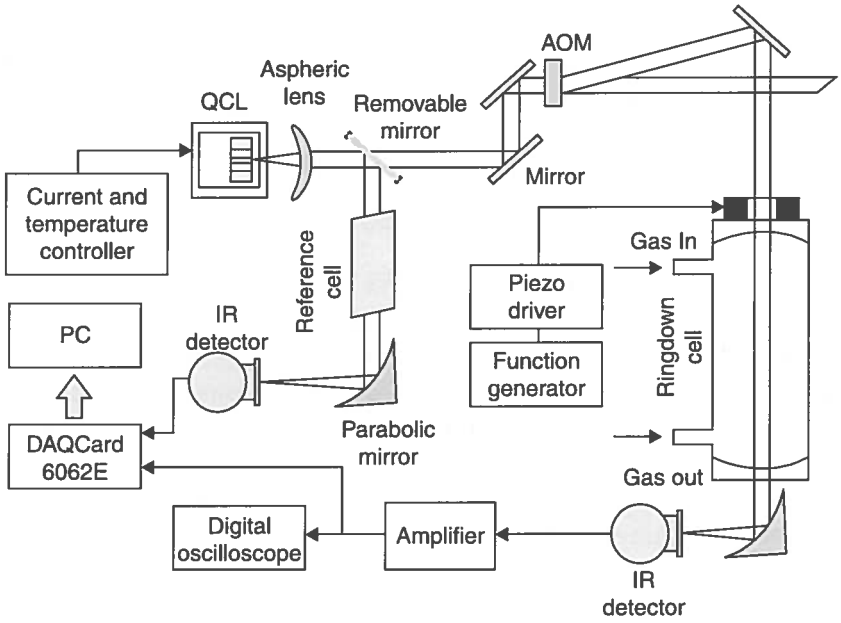


*15.2* A typical CRDS-based sensor platform using an acousto-optic modulator (AOM) as a high speed beam chopper.

pulse powers of only a few times their CW output (Manne *et al.*, 2006). This power limitation can be overcome by locking the cavity to the laser to fill the cavity followed by rapid laser turn off. Alternatively, the cavity can be dithered while a CW laser is scanned slowly (Paldus *et al.*, 2000; Kosterev *et al.*, 2001; Sukhorukov *et al.*, 2006; Rao and Karpf, 2010). A typical CRDS-based sensor platform is shown schematically in Fig. 15.2.

For off-axis ICOS (OA-ICOS), in which the optical sensor system is aligned in such a way that a maximum number of longitudinal and transverse modes is excited within the cavity, the typical optical throughput of the cavity is of the order of $\leq T/2$ (where $T$ is transmission of the cavity mirrors) (Paul *et al.*, 2001). This method is related to absorption spectroscopy using a multipass cell with the significant difference that in ICOS the beams are allowed to overlap on the mirrors after many cavity passes. The principal effect limiting sensitivity is output fluctuations (noise) caused by transmission noise due to the resonant mode structure. One approach for minimizing this noise is to arrange that the laser spots on the mirrors exhibit a circular pattern similar to those of the Herriot multipass cell. If many passes of the cavity take place before any of these spots overlap, interference effects are minimal because the path-length before overlap exceeds the coherence length of the laser. By introducing a small amount of astigmatism, the entire surface of the mirrors can be used (Paul *et al.*, 2001). Another approach for removing mode noise in OA-ICOS is to vibrate the mirrors (Bakhirkin

*et al.*, 2006, Engel *et al.*, 2006). This causes many mode hops to take place within the time required to empty the cavity, effectively averaging out this noise. Thus the trade-off between multipass absorption and ICOS is that in multipass absorption, this mode noise is not present because the spots never overlap, but for similar mirror size and separation, the total path-length can be much greater in ICOS. Since there are no mirror holes in the ICOS cavity configuration to admit and allow the exit of the beam (laser radiation is transmitted through the cavity mirrors) ICOS requires more laser power, which is available with QCL excitation. A medical application of QCL-based OA-ICOS for the measurement of NO and $CO_2$ in exhaled breath was reported in McCurdy *et al.* (2007b). More recently, an OA-ICOS instrument for the measurement of isotope ratios in water in order to obtain information about the role of water in global climate change was reported (Sayres *et al.*, 2009). Furthermore, by combining OA-ICOS with multiple line integrated absorption spectroscopy an ultrahigh sensitivity of 28 ppt for $NO_2$ detection was achieved (Rao and Karpf, 2011).

### 15.2.3 Conventional and quartz-enhanced photoacoustic spectroscopy

CPAS is a well-established trace gas detection method based on the photoacoustic effect. In this method the acoustic wave is created as a result of molecular absorption of laser radiation which is either intensity or wavelength modulated. Such an acoustic wave, when it propagates within the photoacoustic (PA) cell, can be detected by a sensitive microphone (Miklos *et al.*, 2001; Rossi *et al.*, 2005). Instead of a single microphone device, an array of microphones is employed in some CPAS systems to achieve more sensitive results for trace gas detection (Hofstetter *et al.*, 2001b; Elia *et al.*, 2005). In contrast to other infrared absorption techniques, CPAS is an indirect technique in which the effect on the absorbing medium, rather than the direct light attenuation, is analyzed. Therefore, no photodetector is required in the CPAS technique. However, an infrared detector right after the photoacoustic (PA) cell is usually employed for the purpose of monitoring laser power and performing a line locking procedure.

In order to obtain an optimal acoustic signal for amplitude modulated CPAS measurements, the laser modulation frequency is typically selected to match the first longitudinal acoustic resonance of the PA cell, given by the equation $f = v/2L$, where $v$ is the speed of sound and $L$ is the length of cell. The resonance frequencies of PA cells are usually selected to be 1 kHz, the make in order to CPAS technique immune to the intrinsic $1/f$ type noise of the microphone and its pre-amplifier and to low frequency external acoustic noise (da Silva *et al.*, 2004; Pushkarsky *et al.*, 2006b; Lima *et al.*, 2006).

However, the PAS design does not allow a reduction of the photoacoustic cell volume below ~10 $cm^3$.

The detected PA signal ($S_{PA}$) is described by the following equation:

$$S_{PA} = CP\alpha cM, \qquad [15.2]$$

where $C$ is the PA cell constant ($Pa/(Wcm^{-1})$), $P$ is optical power of the laser (W), $\alpha$ is the absorption coefficient of the targeted gas ($cm^{-1}/(molecule\ cm^{-3})$), $c$ is concentration ($molecule/cm^3$), and $M$ is the microphone response (V/Pa).

Ideally, CPAS is a background-free technique because only the absorption of modulated laser radiation generates an acoustic signal. However, background signals can originate from nonselective absorption of the gas cell windows (coherent noise) and external acoustic (incoherent) noise. Therefore, proper isolation of the photoacoustic cell from any mechanical vibrations will result in an improvement of the measured signal-to-noise ratio (SNR). Further CPAS signal enhancement can be achieved by employing a different PAS cell design, such as a resonance photoacoustic cell with two buffer tubes (Rey and Sigrist, 2008) or a ring differential resonance photoacoustic cell (Miklos *et al.*, 1999; Lee *et al.*, 2007). Schematic diagrams of both designs are depicted in Fig. 15.3.

In the two-buffer-tubes PA cell design (Fig. 15.3a), the $\lambda/4$ buffer volume in line with the longitudinal acoustic resonator acts as an acoustic notch filter at the frequency of the resonator, in order to effectively suppress system flow noise (Bijnen *et al.*, 1996). In a differential PA cell (Fig. 15.3b), two identical cylindrical channels are equipped with a microphone, which is placed in the middle of each channel, where the maximum pressure oscillations are observed. Because the CPAS signal is proportional to the absorption coefficient and the laser power, it is possible for both designs to achieve minimum detectable concentrations at the sub-ppb level by selecting the strongest absorption lines of the target gas and by using high power laser sources such as CW $CO_2$ and CO lasers, optical parametric oscillators, fiber amplifiers, or CW DFB-QCLs or EC-QCLs (Bernegger and Sigrist, 1990; Sigrist and Thoeny, 1993; Costopoulos *et al.*, 2002; Pushkarsky *et al.*, 2003, 2006; Webber *et al.*, 2003; Ng *et al.*, 2004; Mukherjee *et al.*, 2008).

A novel approach to the photoacoustic detection of trace gases, utilizing a quartz tuning fork as an acoustic transducer, was first reported in 2002 (Kosterev *et al.*, 2002, 2005b). The key innovation of this new method, named QEPAS, is to invert the common CPAS approach and accumulate the acoustic energy in a sharply resonant piezoelectric transducer with a very high quality factor (Q-factor) of >10 000, rather than in a broadband microphone and low $Q$ (~200) resonant CPAS gas cell. A suitable candidate for such a transducer is a quartz tuning fork (QTF), which is commonly used as a frequency standard in digital clocks and watches. When the QTF is mechanically deformed, electrical charges are generated on its surface

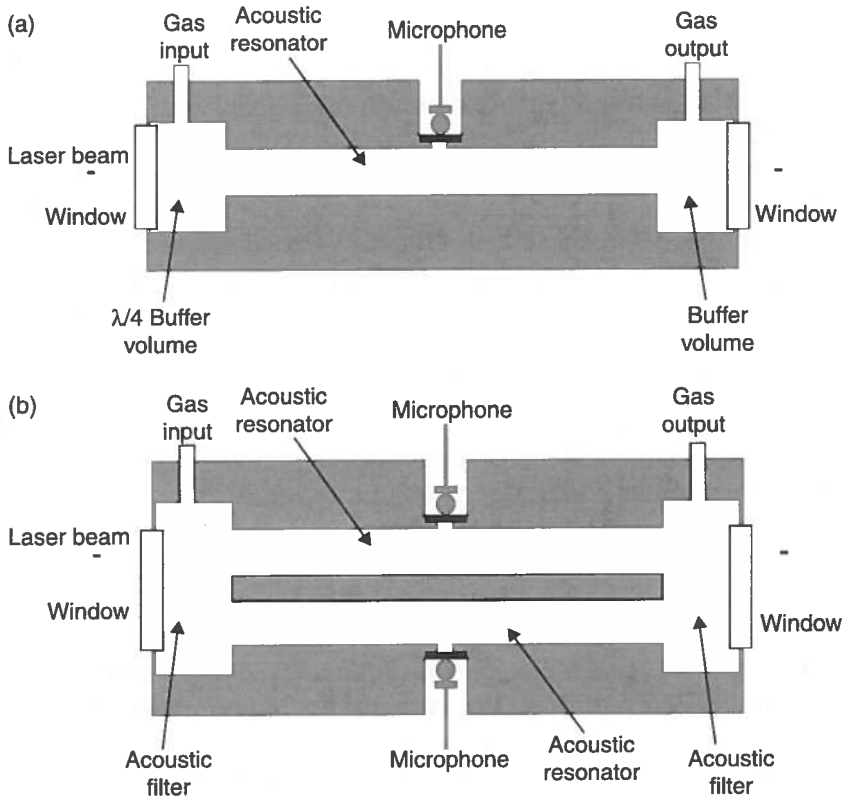


*15.3* (a) Block diagram of a two-buffer-tubes PA cell design and (b) a ring differential resonance PA cell design.

only when the two prongs move in opposite directions (antisymmetric mode of vibration). Thin silver films deposited on the quartz surfaces collect these charges, which can then be measured as either a voltage or a current, depending on the electronic circuit used. In vacuum, QTFs typically resonate at 32 768 ($2^{15}$) Hz which results in a high immunity of QEPAS devices to environmental acoustic noise.

The photoacoustic signal measured by a QEPAS sensor is proportional to:

$$S_0 \sim \frac{\alpha \cdot P \cdot Q}{f_0}, \qquad [15.3]$$

where $\alpha$ is an absorption coefficient, $P$ is optical power, $Q$ is the quality factor of the resonator and $f_0$ is resonant frequency (Kosterev *et al.*, 2005a). The $Q$-factor is dependent upon pressure $p$ and can be expressed as:

$$Q = \frac{Q_{\text{vac}}}{1 + Q_{\text{vac}} \cdot a \cdot p^b}, \qquad [15.4]$$

where $Q_{vac}$ is the quality factor in vacuum and $a$ and $b$ are parameters dependent on a specific quartz TF design (Kosterev *et al.*, 2005b). The pressure corresponding to optimum sensitivity depends upon the vibrational to translational (V-T relaxation) energy conversion cross-section of the gas of interest. In addition, if the V-T relaxation rate is lower than the optical excitation modulation frequency, the amplitude of the optically induced acoustic signal is reduced. This effect is more significant for QEPAS due to the high modulation frequency of ~32.8 kHz. It is more likely to occur with small (2–3 atoms) molecules such as NO, CO, or $CO_2$, which do not have a dense ladder of energy levels to facilitate V-T relaxation. It was experimentally determined in Kosterev *et al.* (2005b) that the optimum pressure for fast-relaxing molecules with resolved optical transitions is <100 Torr, which also ensures Doppler-limited spectral resolution. For slow relaxing gases this optimum pressure is higher and may give a broader linewidth than desirable for the best selectivity.

In a typical QEPAS scheme the laser beam is focused between the QTF prongs as shown in Fig. 15.4a. In this case, the probed optical path is only as long as thickness of the QTF, or ~0.3 mm. Therefore, QEPAS is mostly sensitive to a sound source positioned in a 0.3 mm gap between the prongs. Sound waves from distant acoustic sources tend to move the QTF prongs in the same direction, which results in a zero net piezo-current and makes this element insensitive to such excitation. A configuration shown in Fig. 15.4a can be useful when the excitation radiation cannot be shaped into a near-Gaussian beam, like spatially multimode lasers. The simplest configuration with bare QTF was used in some experiments (Wysocki *et al.*, 2006) and theoretically analyzed in Petra *et al.* (2009). However, the sensitivity can be significantly improved using a configuration as shown in Fig. 15.4b, where a metal tube is added on each side of the QTF to confine the optically generated acoustic vibrations in the gas and increase the effective interaction length between the radiation-induced sound and the QTF (Lewicki *et al.*, 2007a). With respect to the QTF, these tubes can act as an additional acoustic microresonator. Recent experimental studies have revealed that the optimum length for each microresonator tube is somewhere between $\lambda_s/4$ and $\lambda_s/2$ of the propagating sound wavelength ($\lambda_s$) (Dong *et al.*, 2010). Thus, for optimal microresonator configuration, where each microresonator tube is 4.4 mm in length and 0.6 mm in inner diameter, an up-to-30 times improvement in SNR can be observed in comparison to the bare QTF configuration (Dong *et al.*, 2010). Most QEPAS-based sensors utilize a configuration illustrated in Fig. 15.4b. A typical QTF, used in most QEPAS measurements to date, is illustrated in Fig. 15.4c. Other QEPAS spectrophone configurations, such as off-beam QEPAS, are also possible (Liu *et al.*, 2009, 2010). Furthermore, two novel modifications of the QEPAS sensor architecture based on interferometric photoacoustic spectroscopy (Köhring *et al.*, 2011) and resonant

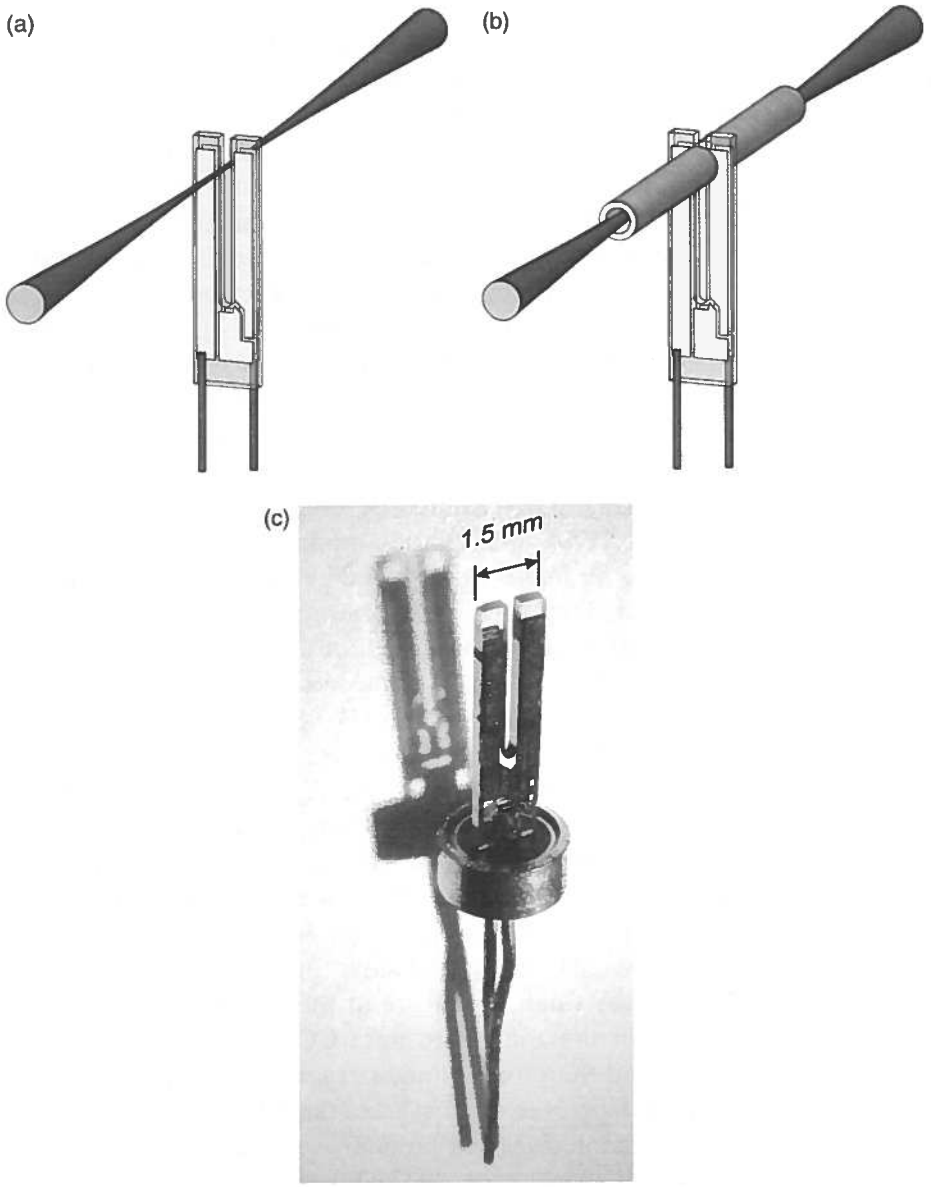


*15.4* QTF-based spectrophones: (a) simplest spectrophone configuration and (b) an improved spectrophone configuration with an acoustic resonator formed by two pieces of rigid tubing (Kosterev, 2010b); (c) a typical quartz tuning fork geometry used in QEPAS trace gas measurements.

optothermoacoustic detection (Kosterev and Doty, 2010) were reported recently.

Like conventional photoacoustic spectroscopy, QEPAS does not require optical detectors and also benefits from the high optical power of laser

source. This feature is especially attractive for gas sensing in the 4–20 μm region, where the availability of high-performance optical detectors is limited, and cryogenic cooling is often required. In spectroscopic measurements based on the QEPAS technique, either the laser wavelength is modulated at $f_m = f_0/2$, or its intensity is modulated at $f_m = f_0$ frequency (where $f_0$ is the QTF resonant frequency), depending on whether wavelength modulation or amplitude modulation technique is used, respectively. In most QEPAS sensor designs, a $2f$ wavelength modulation (WM) spectroscopy has been used (Kosterev and Tittel 2004a, 2004b, 2005a, 2006; Horstjann *et al.*, 2004; Wysocki *et al.*, 2006; Lewicki *et al.*, 2007a; Spagnolo *et al.*, 2010). This technique provides complete suppression of any coherent acoustic background that might be created when stray modulated radiation is absorbed by non-selective absorbers, such as the gas cell elements and the QTF itself. In this case, the noise floor is usually determined by thermal noise of the QTF (Grober *et al.*, 2000). In case of an amplitude modulation (AM) mode the QEPAS sensitivity limit is no longer determined by the QTF thermal noise alone, but by laser power fluctuations and spurious interference features as well. Therefore, the AM mode is often used for detecting large, complex molecules, when individual rovibrational transitions are not resolved and applying the WM technique is not possible (Wojcik *et al.*, 2006; Lewicki *et al.*, 2007b; Bauer *et al.*, 2009, 2010; Kosterev *et al.*, 2010a).

A direct, side-by side comparison of a QEPAS sensor using a QTF enhanced with a microresonator and a CPAS sensor based on a state-of-the-art differential resonance photoacoustic cell (Lee *et al.*, 2007) was demonstrated in Dong *et al.* (2010). Using the $2f$ WM technique, the sensitivities obtained for both QEPAS and CPAS were within the same detection range when both fast (10 ppmv $C_2H_2$ in $N_2$) and slow (pure $CO_2$) relaxing molecules were investigated. A small advantage of the CPAS technique over the QEPAS technique for the analysis of pure $CO_2$, results from a lower modulation frequency and therefore a longer response time ($\tau = Q/\pi f$) of the CPAS spectrophone. However, in most cases the QEPAS detection sensitivity for slow relaxing molecules can be improved by adding a molecular species such as $H_2O$ (Lewicki *et al.*, 2007a; Spagnolo *et al.*, 2010) or $SF_6$ (Kosterev *et al.*, 2005a), which eliminates the V-T relaxation bottleneck.

### 15.2.4 Faraday rotation spectroscopy (FRS)

FRS has been used for many years as a very sensitive and selective technique for the spectroscopic investigation of paramagnetic molecules such as nitric oxide (Litfin *et al.*, 1980; Adams *et al.*, 1984; Ganser *et al.*, 2003; Fritsch *et al.*, 2008; Sabana *et al.*, 2009; Lewicki *et al.*, 2009; Kluczynski *et al.*, 2011), nitrogen dioxide (Dillenschneider and Curl, 1983; Smith *et al.*, 1995),

oxygen (Brecha *et al.*, 1997; So *et al.*, 2011) and hydroxyl radicals (Pfeiffer *et al.*, 1981; Zhao *et al.*, 2011). This technique takes advantage of the dispersion effects of paramagnetic molecules immersed in a longitudinal magnetic field to reveal their unique property to rotate light polarization.

In the presence of a magnetic field, rovibrational transitions of molecules that possess a permanent magnetic dipole moment undergo Zeeman splitting. The magnetic field breaks the degeneracy of the molecular rotation states into $2J + 1$ sublevels labeled by the quantum number $M_J$. Moreover, in the vicinity of a Zeeman-split absorption line of the paramagnetic molecule, circularly polarized components have different wavelength dependent complex propagation constants. Each circularly polarized component interacts either with the $\Delta M_J = +1$ or $\Delta M_J = -1$ NO transition components. For linearly polarized light, which can be considered a superposition of right hand (RHCP) and left hand circularly polarized (LHCP) light, propagation for a distance L through a paramagnetic medium rotates its plane of polarization by an angle $\Theta = \Delta n L \pi / \lambda$, where $\Delta n = n_R - n_L$ is the difference between the refractive index for RHCP ($n_R$) and LHCP ($n_L$), respectively. The change in polarization state can be monitored by placing the gas cell between two nearly crossed Rochon polarizers (RP) and detecting the intensity modulation of the light emerging from the second polarizer, also called an analyzer. For small rotation angles, the polarization rotation and thus the detector signal is directly proportional to the concentration of paramagnetic species inside the cell. The polarization rotation angle can be detected very precisely using an applied modulated magnetic field and phase sensitive detection. Since the polarization rotation, and thus the variation, of the analyzer transmission exist only when the paramagnetic molecules are present in the gas cell, FRS is considered a zero optical background technique.

The basic FRS setup is shown in Fig. 15.5. For low gas concentrations and short optical paths, the magnetic circular dichroism associated with the

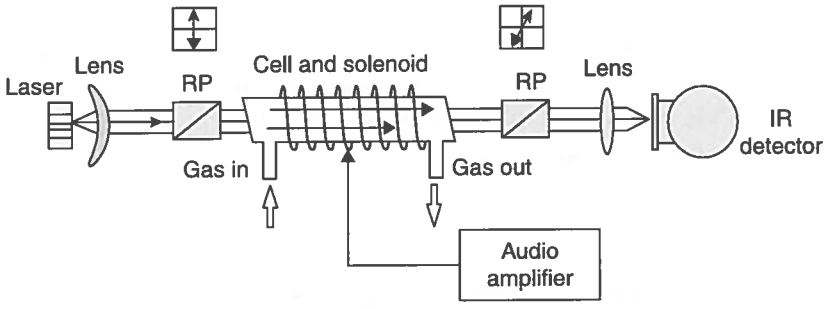


*15.5* Schematic diagram of the 90° FRS scheme. Two RPs are nearly crossed at an angle determined to give the best S/N. Black and grey arrows indicate different light velocities observed for RHCP and LHCP light propagated within the gas cell.

difference between absorption coefficients for RHCP and LHCP light is negligible. In a good approximation, only the magnetic circular birefringence (MCB) signal resulting from the difference between two dispersion curves contributes to the final FRS signal recorded by a low-noise photodetector. This detection method was first reported in the 1980s with a color-center laser source to reduce source noise and improve the sensitivity of the FRS method (Litfin *et al.*, 1980).

For the FRS technique two methods have been used for polarization rotation measurements. The first measurement method, called the 90-degree method, uses two polarizers and a single photodetector to sense the transmitted light intensity (Litfin *et al.*, 1980). In the 90-degree method, laser noise suppression is achieved by nearly crossing the analyzer, thus reducing the amount of laser amplitude noise arriving at the detector. In a situation where the main noise source arises from laser amplitude fluctuations, improved sensitivity through FRS is achieved by reducing laser source noise by a factor larger than the simultaneous reduction of signal. Source noise from laser amplitude fluctuations is at a minimum when the polarizers are exactly crossed and initially increases quadratically upon uncrossing. The FRS signal is null at the exact crossing, but increases linearly upon uncrossing. Therefore, the SNR enhancement can be obtained because the signal is an approximately linear function of the displacement of the analyzer angle from minimum transmitted light, while the noise has a quadratic dependence on the angle. In addition, detector noise is unaffected by the polarizer crossing angle. Quantum or shot noise grows with uncrossing in the same way as the signal. The second measurement method, called a differential detection scheme (Adams *et al.*, 1984) orients the second Rochon polarizer at 45° to the first. This splits the original beam into two equally intense beams of perpendicular polarization; these beams are directed to two balanced detectors and the Faraday rotation is measured as a difference between the two signals. Which method is best depends on several factors: laser power, source noise in the laser, saturation of the absorption, and detector parameters (such as sensitivity, saturation, and linearity). Frequency modulation can be used with any of the FRS methods to approach quantum noise (QN) limited performance (Smith *et al.*, 1995).

The SNR enhancement for both methods is achieved in slightly different ways, but, fundamentally, both are based upon the efficient suppression of laser amplitude noise while maximizing the Faraday rotation signal. Moreover, in both methods, the spectral shape of the FRS signal is the sum of the differences between Zeeman shifted dispersion curves. Depending on the ratio of laser intensity fluctuations to detector noise at the modulation frequency, the SNR can be limited either by detector noise for quiet sources or by polarizer quality for noisier sources. There is an optimum analyzer angle for the 90-degree method, which depends upon detector noise or polarizer quality (Lewicki *et al.*, 2009).

## 15.3 Quantum-cascade lasers (QCL) for trace gas detection

Distributed feedback QCLs (DFB-QCLs) and external cavity QCLs (EC-QCLs) are reviewed followed by broad gain medium designs.

### 15.3.1 Distributed feedback quantum-cascade lasers (DFB-QCL)

In order to utilize QC laser sources for accurate spectroscopic measurements, narrow linewidth and single longitudinal mode operation of the QCLs are essential. The single longitudinal mode operation of QCL devices based on Fabry–Pérot cavities can be achieved either creating a distributed feedback (DFB) at a precisely selected wavelength (Faist *et al.*, 1997; Gmachl *et al.*, 1998; Hofstetter *et al.*, 1999; Hofstetter *et al.*, 2001a; Aellen *et al.*, 2003; Xu *et al.*, 2006) by introducing a periodic grating structure on the top of the QCL waveguide, or by using an external cavity (EC) configuration (Wysocki *et al.*, 2005; Maulini *et al.*, 2005; Wysocki *et al.*, 2008).

The single-mode wavelength $\lambda_B$ of the DFB laser is determined by the Bragg reflection condition $\lambda_B = 2n_{\text{eff}}d$, where $n_{\text{eff}}$ is the effective refractive index of the waveguide and $d$ is the period of the diffraction grating. Light satisfying this condition is strongly reflected off the grating and is selected for laser action. Wavelength tuning of the DFB lasers is mainly achieved by the temperature dependence of the refractive index and can be obtained by changing the temperature or by varying the injection current (Joule heating) of the laser. By increasing the temperature of the laser structure, the effective refractive index $n_{\text{eff}}$ increases resulting in a higher emitted wavelength (lower emitted frequency). For state-of-the-art DFB-QCLs, typical current and temperature tuning coefficients are –0.01 $\text{cm}^{-1}$/mA and –0.16 $\text{cm}^{-1}$/K, respectively. This results in a total spectral range of 4 to 5 $\text{cm}^{-1}$ and 15 to 20 $\text{cm}^{-1}$ for maximum current and temperature tuning ranges, respectively. However, an increase of the QCL temperature during the tuning process can result in a decrease of the output optical power, which must be avoided for power dependent spectroscopic techniques such as CPAS or QEPAS. Therefore, DFB-QCLs are typically designed for operation at a single target frequency with a practical tuning range of few $\text{cm}^{-1}$ (Yu *et al.*, 2005). Moreover, they are usually used in trace gas detection and quantification of small molecules with narrow, well resolved rotational-vibrational lines (Bakhirkin *et al.*, 2006; McCurdy *et al.*, 2007a; Grossel *et al.*, 2008).

The spectral tuning range of DFB–QCLs was recently extended by fabricating an array of 32 DFB lasers that were grown on a single chip and driven individually by a microelectronic controller (Lee *et al.*, 2007). The active region of each laser consists of 35 stages based on bound-to

continuum design centered at 9 μm. The DFB-QCLs array operating in a pulsed mode offers a wide continuous spectral tuning range of 85 $cm^{-1}$ from ~1064 $cm^{-1}$ (9.4 μm) to 1149 $cm^{-1}$ (8.7 μm) (Lee *et al.*, 2009a). The continuous spectral coverage of the DFB-QCLs array is achieved by small range temperature tuning to eliminate any spectral gaps. The lasers can be heated locally by changing dc current value delivered to the individual laser or heated by changing the temperature of the heatsink on which the laser array is mounted. The former process can reach the desired wavelength in milliseconds, while the latter process requires several seconds. The DFB QC lasers linewidth, estimated to be ~0.01 $cm^{-1}$ in pulsed operation and ~0.001 $cm^{-1}$ in CW operation, is significantly better than the resolution offered by a typical 'bench top' FTIR (~0.1 $cm^{-1}$). Furthermore, the same group fabricated an ultra-broadband DFB-QCLs array, consisting 24 DFB-QCLs which have a heterogeneous cascade structure based on two bound-to-continuum designs centered at 8.4 and 9.6 μm (Lee *et al.*, 2009b). This resulted in an overall frequency tuning range of 225 $cm^{-1}$, centered at 1150 $cm^{-1}$ (~8.7 μm). The 24 single-mode DFB-QCLs array has proven its capability as a spectroscopic source for sensitive detection of different broadband absorbing molecular species including isopropanol, methanol, and acetone (Lee *et al.*, 2007).

Nowadays a single frequency CW DFB-QCLs can provide >100 mW of optical power at room temperature (Yu *et al.*, 2005). Recently, a single-mode emission of more than 150 mW output power was demonstrated for CW RT (room temperature) 7.74 μm DFB-QCL devices fabricated with a buried grating geometry (Troccoli *et al.*, 2010). Approximately 100 mW of optical power was demonstrated for 3.8 W of electrical power consumption with a DFB device at a TEC accessible temperature of 263 K (Wittmann *et al.*, 2009). A state-of-the-art 2.4 W TEC CW operated DFB-QCL was recently demonstrated at 4.8 μm (Lu *et al.*, 2011). High power single mode operation and 10% peak wall plug efficiency from one facet at 298 K was obtained. This was achieved by a surface-plasmon coupling mechanism as well as a combination of high-reflection and antireflection dielectric coatings. Moreover, high power, CW, TE-cooled DFB-QCLs are also commercially available (e.g., www.3–5lab.fr, www.alpeslasers.ch, www.atoptics.com, www.hamamatsu.com, www.nanoplus.com, www.maxion.com).

### 15.3.2 External cavity quantum-cascade lasers (EC-QCL)

Another approach to achieve single frequency operation is to integrate a Fabry–Pérot QCL with broadband gain medium (Faist *et al.*, 2001; 2002) into an EC configuration (Maulini *et al.*, 2004, Maulini *et al.*, 2005; Wysocki *et al.*, 2005; Maulini *et al.*, 2006). The main advantage of using EC-QCL sources, as

compared to DFB-QCLs and DFB-QCL array devices, is primarily due the fact that they have a much wider wavelength tuning range which is only limited by the effective bandwidth of the QCL gain medium. Hence, EC-QCL sources are better choices to perform simultaneous spectroscopic measurements of multiple chemicals species or broadband absorbing molecular species detection. The implementation of the near RT and wide gain profile pulsed Fabry–Pérot QCLs into external cavities resulted in a wide frequency tuning range of 432 $cm^{-1}$ (Hugi, 2009, Hugi, 2010) and ~200 $cm^{-1}$ in CW mode (Maulini, 2006; Pushkarsky, 2006a; 2006b; Wysocki, 2008; Wittmann, 2008; Hugi, 2009, 2010).

An EC-QCL system consists of three main optical elements: a QCL gain chip, an aspherical lens to collimate laser light, and a diffraction grating which acts as a wavelength-selective filter. The two most commonly used configurations for grating-coupled EC systems which employ a QCL as a gain medium are the Littman-Metcalf (Phillips, 2007) and the Littrow configurations (Arnold, 1998). Each type of EC configuration has its special advantage, which makes it best suitable for a certain type of applications. General performance and wavelength tuning behavior of QC lasers in Littrow and Littman-Metcalf cavity configurations were studied in detail in Guipeng (2002), demonstrating similar wavelength tuning properties for both configurations. For trace gas detection, Littrow configured external cavity quantum-cascade laser (EC-QCL) systems (Lewicki *et al.*, 2007b; Wysocki *et al.*, 2008; Karpf and Rao 2009; Scherer *et al.*, 2009; Tsai and Wysocki 2010; Spagnolo *et al.*, 2010) are more often employed than Littman-Metcalf systems (Phillips *et al.*, 2007). In the Littrow configuration, the first-order diffraction beam is directly feedback to the laser, which results in obtaining an optimal condition for the QCL tuning range. Due to the double diffraction from the grating the Littman-Metcalf configuration offers narrower linewidth than the Littrow configuration at the expense of both optical power and spectral tuning range due to decreased grating feedback strength.

In a Littrow configured EC-QCL a coarse wavelength tuning is achieved by varying the angle of the diffraction grating. This will result in discrete tuning jumps between the internal Fabry–Pérot cavity modes of the laser chip or between EC modes. Both cavity modes are separated by $\nu \approx 1/2nL$, where $L$ is the cavity length and $n$ is the refractive index of the cavity medium. In order to achieve continuous, fine mode-hop free tuning, the cavity length and grating angle must track each other. The mode-hop free tuning ability and tuning range is significantly improved when an anti-reflection (AR) coating is implemented at the front facet of the Fabry–Pérot QCL. In this case, the effect of the optical cavity formed by the laser itself is eliminated and stronger feedback from the diffraction grating to the laser chip is achieved. Furthermore, a high reflection coating

deposited on the back facet improves the optical gain within the QCL gain structure.

Several interesting schemes of fine wavelength tuning based on EC systems were demonstrated in the following publications (Maulini *et al.*, 2005; Wysocki *et al.*, 2005; Pushkarsky *et al.*, 2006a, 2008; Day, 2010). In the first scheme, a fine wavelength tuning was achieved by varying the grating angle and the laser current or the heatsink temperature at the same time (Maulini *et al.*, 2005). However, this configuration suffers from mode hopping due to the lack of control for the EC length when the laser was tuned. Thus, the laser jumped between modes separated by $\nu$ ~0.05 $cm^{-1}$, which was very hard to observe with 0.125 $cm^{-1}$ maximum resolution of FTIR spectrometer. Wysocki *et al.* at Rice University demonstrated an EC-QCL architecture that employed a piezo-activated cavity mode tracking system that provided independent control of the EC and the QCL lengths as well as the diffraction grating angle for mode hop free operation (Wysocki *et al.*, 2005; 2008). The wavelength tuning is realized by simultaneous control of all three system features significant for the mode tracking: grating angle, EC length, and the laser current. Another approach enabling continuous mode hop free tuning of the EC-QCL system was achieved by simultaneously adjusting the grating angle and periodically varying the laser injection current to achieve a continuous shift of the Fabry–Pérot comb of the gain chip (Pushkarsky *et al.*, 2006b). In this method the laser current value is selected to have one of the Fabry–Pérot modes of the gain chip exactly coincide with the desired output frequency as the laser is tuned. To support single-mode operation at every selected grating angle, fine adjustments of the EC length was achieved by the grating mounted on the rotational stage operated by a piezoelectric linear translator. To minimize the effect of spectral mode hops across the modes of the EC, a very long EC length of 1 m was used, resulting in Fabry–Pérot mode spacing of 0.005 $cm^{-1}$.

An interesting scheme based on a miniature EC system wavelength tuning has been implemented by Daylight Solutions (www.daylightsolutions.com). The Daylight Solutions EC-QCL consists of a 25 mm long optical cavity length, miniature grating tuning mechanism, and integrated current and temperature controls. The laser chip facet facing the grating is AR coated, while the output facet is left uncoated. The radiation from both facets was collimated with a pair of AR coated aspheric lenses. Wavelength tuning of these systems is realized with a Littrow grating angle controlled by means of a stepper motor and an integrated absolute optical encoder with microprocessor-based closed loop controller (Pushkarsky *et al.*, 2008; Caffey *et al.*, 2010). The grating motion is mechanically constrained to follow a trajectory allowing for the simultaneous tuning of the diffraction grating angle and the laser cavity length, thereby constraining the EC mode to coincide with the wavelength selected by the grating. Another miniature EC-QCL from

Daylight Solutions using a microelectromechanical systems (MEMS)-based grating for fine adjustment of the laser wavelength within limited tuning range was recently demonstrated in Weida *et al.*, (2010). The MEMS-based EC-QCL system, inside a 2 cc volume high heat load (HHL) laser 2 cc in volume, will offer a precise mode hop free tuning within approximately $\pm$ 8 $cm^{-1}$ from its center wavelength. This tuning range is sufficient to perform high-resolution gas-phase spectroscopy of molecules with narrow spectral features.

### 15.3.3 Quantum-cascade laser broad gain medium designs

Several schemes of broad gain QCL designs have been demonstrated by several groups. The first scheme employs at least two stacks of cooperative quantum-well active regions of dissimilar intersubband optical transitions, leading to a heterogeneous cascade over a very wide spectral range (Gmachl *et al.*, 2001). Each active region stage needs to be specially engineered to achieve an optimally flat gain spectrum over the emission range of interest. For two active regions designed to emit at 5 and 8 μm, a supercontinuum emission of the laser from 6 to 8 μm was achieved and demonstrated for the first time in Gmachl *et al.* (2002).

The second scheme is based on a single bound-to continuum active region design (Faist *et al.*, 2002) or heterogeneous quantum-cascade structure based on two bound-to-continuum designs (Maulini *et al.*, 2006; Wittmann *et al.*, 2008). In a bound-to continuum design the radiative transitions occur between a single upper state and closely spaced sublevels (quasi-miniband) of final lower states. Therefore, the oscillator strength that describes the strength of the transition is not concentrated in a single radiative transition but is extended over multiple transitions, giving rise to broad gain spectrum of the QCL. The first implementation of a Fabry–Pérot QC laser based on the bound-to-continuum design coupled to an EC was demonstrated in 2004 exhibiting a broad tuning range of 150 $cm^{-1}$ at 10 μm (Maulini *et al.*, 2004). The first heterogeneous cascade QCL based on two bound-to-continuum active region designs, exhibiting a gain spectrum width (FWHM) as large as 350 $cm^{-1}$, was demonstrated in 2008 (Wittmann *et al.*, 2008). Each active region of this heterogeneous laser structure was designed to emit radiation at 8.2 and 9.3 μm wavelengths. A coarse frequency tuning from 1013 $cm^{-1}$ (9.87 μm) to 1305 $cm^{-1}$ (7.66 μm) and from 1045 $cm^{-1}$ (9.57 μm) to 1246 $cm^{-1}$ (8.02 μm) was achieved in pulsed and CW operation, respectively for the laser implemented into a Littrow type EC-QCL configuration and operated at RT. The pulsed tuning range of 292 $cm^{-1}$, which is 25 % of the laser center frequency, was the recorded value at that time.

The ultra-broad gain quantum-cascade laser was developed using five distinctive substacks (ST) based on bound-to continuum design to form the active region (Hugi *et al.*, 2009). In order to obtain flat gain spectrum and achieve a gap free tuning over the whole spectral emission range, the gain of each substack of the active region, centered at 7.3, 8.5, 9.4, 10.4, and 11.5 μm wavelength was properly optimized. After coupling the laser in a Littrow EC setup a total wavelength coverage from 7.6 μm to 11.4 μm (1309–878 $cm^{-1}$), with a peak optical output power of 1W and an average output power of 15 mW at RT has been demonstrated. The obtained frequency tuning of 432 $cm^{-1}$ results in a record tuning of 39.5% around the laser center frequency. In addition, this design scheme is not limited to the specific wavelength and can be customized to access other spectral region of mid-IR radiation. Recent advances in broadly tunable EC-QCL systems comprising different bound-to continuum active region designs are demonstrated in Hugi *et al.* (2010).

Recently, an interesting approach to the fabrication of homogeneous broad gain QCLs based on dual upper state design was demonstrated by researchers from Hamamatsu (Fujita *et al.*, 2010). In their design, the electrons are injected into the higher upper state 4 of active regions, via resonant tunneling from ground state, and then, they are quickly distributed in the two upper laser states by optical-phonon scattering or by electron-electron scattering. The broad and symmetric optical gain is achieved not only due to $E_{43}$ ~ 20 meV in energy difference, between two 4-to-2 and 3-to-2 radiative transition levels, but also due to equal oscillator strengths of the transitions from both upper laser states to the lower common laser state. The dual upper state-based QCL devices exhibit a homogeneously wide electroluminescence spectra of >330 $cm^{-1}$ and insensitivity to the temperature or voltage changes. In CW operation at 300 K, the optical output laser power was 152 mW.

Another example of broadband QCL gain medium is based on 'continuum-to-bound' active region design, where the two lower injector states are strongly coupled with the upper laser state (Yao *et al.*, 2010a). Ultra-strong coupling between the injector states and the upper laser state improves electron injection efficiency, reduces the transit time from injectors to the active region, and provides three laser transitions that are separated by an energy of ~20 meV. The radiative transitions from these three coupled states contribute to a large gain spectrum width of ~250 $cm^{-1}$ full width at half maximum, which enables EC tuning of the lasers over 200 $cm^{-1}$. Recently, the same group demonstrated a 'continuum-to-continuum' quantum-cascade laser design (Yao *et al.*, 2010b), where optical transitions from four strongly coupled upper states to lower laser states contribute to the gain spectrum. In this design, a broad gain bandwidth of over 400 $cm^{-1}$ has been demonstrated in the 4–5 μm wavelength region.

## 15.4 Specific examples of QCL-based sensor systems

Various applications of EC-QCL-FRS and DFB-QCL-QEPAS are described in the following subsections.

### 15.4.1 Faraday rotation spectroscopy for ultra-sensitive detection of nitric oxide and nitrogen dioxide

FRS is a well-recognized detection technique that is highly sensitive and selective to paramagnetic molecules only. Therefore, the FRS technique is well suited for atmospheric detection of prominent air pollutants (NO, $NO_2$) or for exhaled breath analysis (NO) (Mürtz and Hering, 1999). This is because interference from diamagnetic species, such as water and carbon dioxide, is effectively eliminated. Moreover, a biogenic NO released from human sweat, has also been monitored with the FRS technique (Ganser *et al.*, 2004).

An access to the optimum for FRS measurements molecular transitions of the paramagnetic species of interest enable to perform accurate quantitative measurements at or below the parts-per-billion by volume (ppbv) levels (Lewicki *et al.*, 2009; Kluczynski *et al.*, 2011; Zaugg *et al.*, 2011). For sensitive FRS detection of NO the best choice is the $Q_{3/2}(3/2)$ molecular transition at 1875.81 $cm^{-1}$ (5.33 μm) (Ganser *et al.*, 2003). Tuning to this line was made possible by employing a widely tunable CW TE-cooled EC-QCL as a spectroscopic source (Wysocki *et al.*, 2008). The total EC-QCL frequency tuning range, between 1825 $cm^{-1}$ (5.48 μm) and 1980 $cm^{-1}$ (5.05 μm), allows most of the lines within the fundamental absorption band of NO at 5.2 μm to be targeted with a single laser source.

The experimental arrangement of the prototype FRS platform shown in Fig. 15.6 was transported and operated at three different laboratory locations. A widely tunable 5.3 μm EC-QCL with high-resolution MHF wavelength tuning capability was used as the spectroscopic source. In this experiment, the laser was operated in a CW mode at –20°C and provided a maximum output power of 2.9 mW at the wavelength coincident with the target NO line. MHF tuning of up to 2.5 $cm^{-1}$ permitted high-resolution spectroscopy anywhere within the tuning range.

The collimated EC-QCL beam (4 mm in diameter) was split by a ZnSe wedge into two independent optical paths. In the main path the laser beam propagated through a 50 cm long optical gas cell located inside a 44 cm long solenoid. The gas cell was placed between two nearly crossed $MgF_2$ RPs (the extinction ratio for both polarizers is $\xi < 10^{-5}$). When a longitudinal magnetic field was applied, the linearly polarized QCL beam experienced a Faraday rotation of the plane of polarization as a result of the interaction with paramagnetic NO molecules. The Faraday rotated light, passing through a second polarizer, was detected by either a mid–infrared

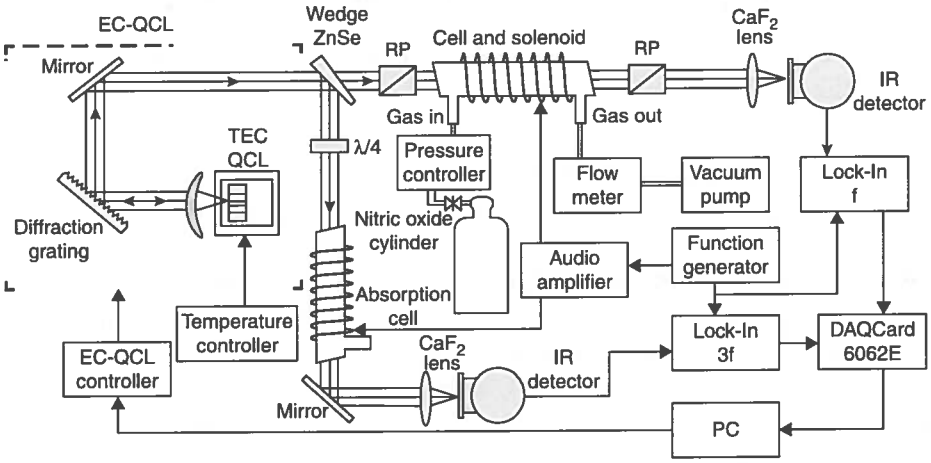


*15.6* Schematic diagram of an EC-QCL-based FRS experimental setup. RP – Rochon polarizer, λ/4 – quarter wave plate, PC – personal computer (Lewicki *et al.*, 2009).

thermoelectrically cooled mercury-cadmium-telluride (MCT) photodetector or liquid-nitrogen cooled indium-antimonide (InSb) photodetector. The solenoid current was driven at $f_m$ = 950 Hz with a commercial high power audio amplifier (QSC audio model: RMX850). To minimize power requirements for driving the reactive load of the solenoid at ~1 kHz, a series resonant circuit was constructed matching the modulation frequency ($f_m$). The modulated Faraday rotation resulted in the AC amplitude modulation of the transmitted light intensity, which was detected using a phase sensitive lock-in detection at the frequency $f_m$. For calibration of the FRS spectrometer, two cylinders containing a mixture of 10 ppmv and 96 ppbv of NO in $N_2$ were used. The system gas flow rate was set to ~300 ml/min.

The second optical branch of the sensor was used as the reference channel for frequency control of the EC-QCL. The initial linear polarization of the laser radiation was transformed into circular polarization by passing it through a quarter wave-plate (λ/4) (Alphalas, tunable quarter wave-plate). The beam was directed through a 20 cm absorption gas cell filled with a mixture of 5% NO by volume in air at 25 Torr. The reference absorption cell was placed inside a 10-cm long solenoid that produced an axial magnetic field. The second solenoid was a part of the series RLC circuit formed with the main solenoid, and was supplied from the same high power audio amplifier. In the presence of alternating magnetic field, a Zeeman modulation signal resulting from the interaction between circularly polarized light and NO molecules through magnetic circular dichroism was observed. The Zeeman signal was recorded by a thermoelectrically cooled MCT photodetector

and demodulated by a second lock-in amplifier at the third harmonic of $f_m$. Zeeman detection at the third harmonic, although providing a lower SNR than the conventional 1st harmonic detection, is less sensitive to the electromagnetic interference induced in the system at the fundamental modulation frequency (electromagnetic interference induced in the signal interconnects, front-end electronics, etc.). The zero-crossing of the third harmonic signal is used to lock the EC-QCL frequency to the peak of the optimum $Q_{3/2}(3/2)$ molecular transition of NO at 1875.81 $cm^{-1}$ (5.33 μm). This active wavelength locking technique significantly reduces frequency drift and improves the long-term system stability.

A series of experiments were performed to determine the optimum magnetic field strength, sample gas pressure, and the analyzer offset angle. The best result for the FRS signal amplitude was obtained experimentally at a pressure of 40 Torr and for a magnetic field of B = 110 $Gauss_{rms}$, measured inside the main magnetic coil. The best SNR for a lock-in time constant of 1 sec occurs an angle offset of about 7° from the crossed position when using a thermoelectrically cooled MCT photodetector (with area of 1 $mm^2$ and peak detectivity of $D^* > 2\times10^{10}\,\mathrm{cm}\sqrt{\mathrm{Hz}}\,/\,\mathrm{W}$ at 5 μm). However, for better long-term stability of the system, it is preferable to work with smaller offset angles. For an experimental demonstration of the effect of improved photodetector performance on the system SNR, measurements using a 1 mm diameter liquid-nitrogen cooled InSb photodetector with a specified peak detectivity at 5 μm of $D^* > 1\times10^{11}\,\mathrm{cm}\sqrt{\mathrm{Hz}}\,/\,\mathrm{W}$ were performed. For this case, the optimum analyzer offset was found to be 2–3° from its crossed position.

The high-resolution magnetic rotation spectra of nitric oxide acquired with two different photodetectors for a certified reference gas mixture of 96 ppbv of NO in nitrogen are depicted in Fig. 15.7. Both spectra were recorded under the same experimental conditions ($p$ = 40 Torr, $B$ = 110 $Gauss_{rms}$), and show only the two strongest $Q_{3/2}(3/2)$ and $Q_{3/2}(5/2)$ molecular transitions at 1875.81 $cm^{-1}$ (5.33 μm) and 1875.72 $cm^{-1}$, respectively. For the MCT detector (Fig. 15.7a), a 1$\sigma$ minimum detection limit (MDL) of 4.3 ppbv was obtained for NO concentrations with a 1 s lock-in time constant and analyzer offset angle of $\alpha$ = 7°. A significantly improved detection limit was obtained with the $LN_2$ cooled InSb photodetector, resulting in a 1$\sigma$ MDL of 380 ppt for the same 1 sec lock-in amplifier time constant and analyzer offset angle of 3° (Fig. 15.7b). Equivalent minimum detectible fractional absorptions of 6.7 × $10^{-7}$ and 5.9 × $10^{-8}$ were obtained for the MCT and InSb detector, respectively. All of these results were achieved with rather short active optical paths of 44 cm. Usually to obtain similar detection limits with standard laser absorption spectroscopic techniques, significantly longer optical path lengths, ranging from several to hundreds of meters, are required (Moeskops *et al.*, 2006; McManus *et al.*, 2006).

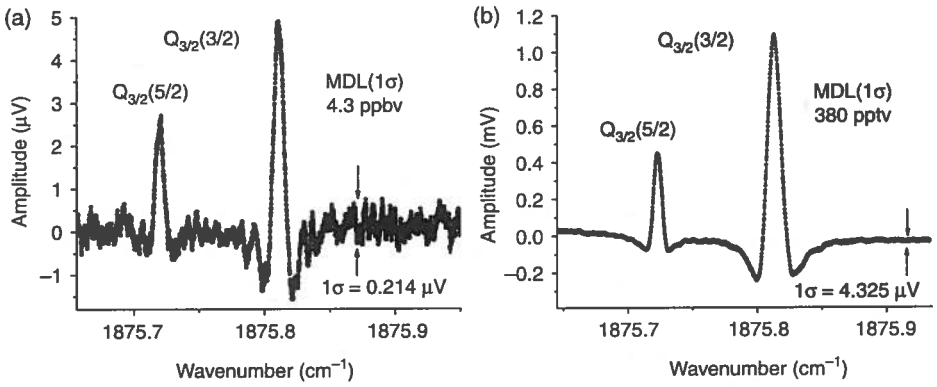


*15.7* (a) Faraday rotation spectrum of $Q_{3/2}(3/2)$ and $Q_{3/2}(5/2)$ transitions of nitric oxide centered at 1875.8 $cm^{-1}$ measured with a thermoelectrically cooled MCT photodetector and (b) with a liquid nitrogen cooled InSb photodetector (Lewicki *et al.*, 2009).

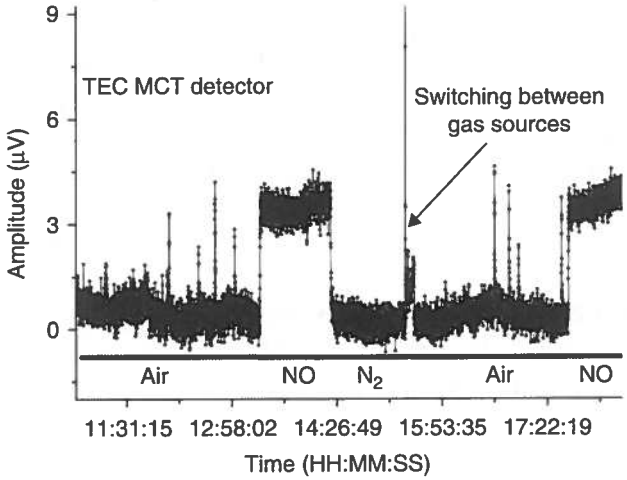


*15.8* Long-term NO concentration measurements performed with active laser frequency locking to the NO absorption line at 1875.81 $cm^{-1}$ (5.33 μm) with MCT photodetector. Acquisition every 3 s, TC = 1 s.

In order to perform continuous and long-term autonomous operation of the FRS sensor platform on the selected molecular transition (1875.81 $cm^{-1}$) an active EC-QCL frequency locking technique was implemented. To prevent detuning of the laser from the resonance with the NO $Q_{3/2}(3/2)$ transition, a computer-based active feedback loop provides simultaneous control of the three independent laser parameters: the EC length, the diffraction grating angle and QCL injection current. The atmospheric data, measured alternately with a certified mixture of 96 ppbv NO in $N_2$ and pure $N_2$, are shown in Fig. 15.8 as an example for FRS system's capability for continuous

unattended operation. During measurements of the air, a number of sharp peaks of NO concentration, primarily related to automobile activity, were detected. The data were acquired every 3 s with a lock-in time constant of 1 s by using the RT MCT detector (7° analyzer offset angle).

The MDL observed in the absorption line-locked mode is about two times higher than the MDL determined from the spectral measurements in Fig. 15.7. This increase in the observed MDL value is related to the limited precision of a relatively slow computer-based active feedback control of the laser wavelength. A more important issue is an offset from the zero signal and a baseline drift which can be caused by electronic pick-up of the 950 Hz modulation current, into the detection system, the laser driver system, or both. For a system limited by photodetector noise a decrease of the analyzer offset is affecting the SNR. In addition, if the analyzer angle is too big the laser intensity variations will be incident on the detector and thus appear in the FRS signal. Therefore, it is necessary to select the conditions that provide optimum long-term stability and a sufficient MDL required for the particular application. Thus, better long-term performance is achieved by using smaller polarizer angle offsets.

The effective suppression of a slow system drift and extended long-term stability was achieved for an analyzer offset angle of 4°. For this condition, the Allan variance calculated for recorded over ~9 h time series of nitrogen shows exceptional stability of the system, which allows for averaging times of up to ~4000 s. Allan variance plots were first introduced by Werle (Werle *et al.*, 1993) for the assessment of LAS-based instrument performance. Moreover, the long-term drift problem can be also eliminated by: (1) tracking down and eliminating ground loops and electromagnetic pick-up, which cause the modulation of the laser by the magnet current, or (2) scanning the laser over the line and averaging series of acquired scans. The final signal, proportional to NO concentration, would be obtained by least squares fitting the amplitude parameter of the known lineshape (as shown in Fig. 15.7) to the observed average traces.

The FRS sensor was configured as a transportable platform with a fully automatic gas handling and periodic calibration system for a long-term field test of NO monitoring applications. A fully automated and autonomous EC-QCL Faraday rotation spectroscopic sensor system was deployed at the Beijing test site for continuous atmospheric NO air-quality monitoring during 2008 Olympic Games.

Furthermore sensitive detection of $NO_2$ at single ppb concentration levels was performed based on a double pass configured Faraday rotation spectrometer, which is a modified version of the NO FRS system illustrated in Fig. 15.6. $NO_2$ is also a major atmospheric pollutant and is mostly emitted by internal combustion engines (e.g., car, trucks, or jet engines) and thermal power plants. The $NO_2$ FRS sensor employs a widely tunable CW EC-QCL

(Daylight Solutions, Model 21062-MHF-012) operating at a temperature of 18°C and providing a maximum optical power of 150 mW. The available EC-QCL frequency tuning range, between 1538.3 $cm^{-1}$ and 1703.3 $cm^{-1}$, covers the entire fundamental $\nu_3$ band of $NO_2$, centered at ~1600 $cm^{-1}$. The optimum $4_{41} \leftarrow 4_{40}$ Q-branch $NO_2$ transition at 1613.25 $cm^{-1}$ was located within the available MHF frequency tuning range between 1600 $cm^{-1}$ and 1650 $cm^{-1}$. To our best knowledge, this is the first time that $NO_2$ was detected at this transition with an EC-QCL-based FRS technique.

For the selected $NO_2$ absorption line at 1613.25 $cm^{-1}$ the optimum pressure, with respect to the highest SNR for the FRS measurements, was selected to be 30 Torr. An optimum analyzer angle of 3° from the crossed position was found to be a trade-off between the TE-cooled MCT detector signal and laser noise level transmitted by the analyzer. The experimentally determined optimum magnetic field is ~200 Gauss (rms), which corresponds to a solenoid current of ~6 A (rms). The FRS spectrum of the Q-branch $NO_2$ transitions in the fundamental $\nu_3$ band was recorded for single pass configuration of the sensor and plotted for comparison with a HITRAN simulated spectrum (Fig. 15.9a). As a reference, a calibration mixture of 2 ppmv $NO_2$ in $N_2$ at the pressure of 30 Torr was used. The analyzer angle is set to 2° from the totally crossed position. The laser frequency was mod-hop free tuned over ~0.8 $cm^{-1}$ by applying a 1 mHz sine wave with an amplitude of 60.5 V to the piezo element. The spectrum was recorded with a lock-in amplifier time constant set to 1 s. The mismatch of the transition frequencies between the simulated and measured spectrum is caused by a slight non-linearity in the frequency tuning of the EC-QCL (Zaugg *et al.*, 2011).

The FRS signal of $NO_2$ at the preferable $4_{41} \leftarrow 4_{40}$ transition (1613.25 $cm^{-1}$) for double pass configuration was acquired over a narrow frequency spectral range of ~0.04 $cm^{-1}$ and illustrated in Fig. 15.9b. For an optimum system pressure of 30 Torr and 2 ppmv of $NO_2$ concentration, a minimum sensitivity was found to be 1.1 ppbv ($1\sigma$) for a 1 s lock-in time constant. However, for laser frequency locked to the $NO_2$ transition at 1613.25 $cm^{-1}$, a slow drift and FRS signal fluctuations during the long-term measurements limit the minimum detection to ~2.5 ppbv. Similar to NO FRS measurements, the observed fluctuations are likely caused by electrical noise generated in the FRS system (ground loops and electromagnetic coupling between coil and detector), since the FRS system is insensitive to optical noise and no additional background signal is present. Further improvement in the SNR can be achieved by using better quality polarizers, more sensitive photodetectors, or by reducing the system noise. In addition, as was shown here, the improved detection limit of the FRS signal can be achieved by increasing the active path-length.

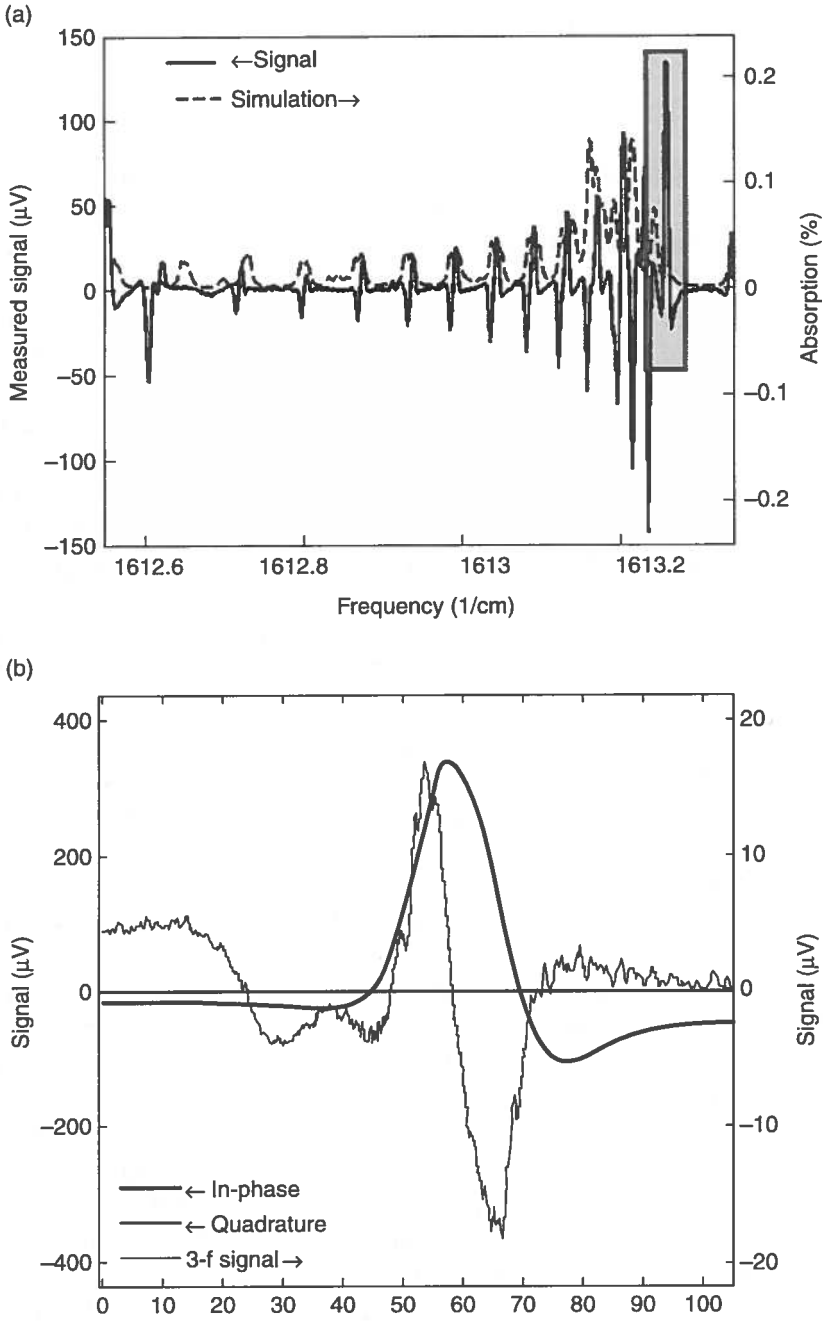


*15.9* (a) $NO_2$ FRS signal within Q-branch of the fundamental $\nu_3$ band for a single pass system configuration; (b) FRS signal of $NO_2$ at the optimum $4_{41} \leftarrow 4_{40}$ transition at 1613.25 $cm^{-1}$ (6.2 μm) for double pass system configuration. 2 ppm $NO_2$ at 30 Torr.

### 15.4.2 Real time ammonia detection in exhaled human breath using a 10.4 μm DFB-QCL-QEPAS-based sensor

Exhaled breath is a mixture of more than four hundred molecules, some of which are present at parts-per-billion (ppb) or even parts per trillion (ppt) concentration levels (Dweik and Amann, 2008). Moreover, some of the exhaled molecules can provide a unique breath profile of the health condition and therefore can be used as biomarkers for the identification and monitoring of various types of human diseases or wellness states (Risby and Tittel, 2010). Currently, the standard analytical chemistry instrumentation used for human breath analysis is gas chromatography, based on various detection methods such as flame ionization detection (Kneepkens *et al.*, 1994; Phillips *et al.*, 1991), mass spectrometry (Cheng and Lee, 1999), ion mobility spectrometry (Westhoff *et al.*, 2009), or selected ion flow tube mass spectrometry (Smith and Španěl, 2005). However, sensitive, real time detection of molecular species in breath samples, was recently demonstrated with laser-based breath analyzers employing different spectroscopic techniques (McCurdy *et al.*, 2007b; Roller *et al.*, 2007; Mürtz and Hering, 2008; Shorter *et al.*, 2010; Thorpe *et al.*, 2008). In this section, a quantum-cascade laser-based optical breath sensor for ammonia detection will be described. By monitoring ammonia concentration levels in exhaled breath, a fast, non-invasive diagnostic method for treatment of patients with liver and kidney disorders is feasible.

The schematic diagram of the ammonia breath sensor architecture based on a QEPAS technique (Kosterev *et al.*, 2002 and Tittel; Kosterev *et al.*, 2004) is depicted in Fig. 15.10. The QEPAS system employs an ultra-small piezoelectric QTF enhanced with optimal microresonator tubes design, where inner diameter and the length of each tube are 0.6 mm and 4.4 mm, respectively (Dong *et al.*, 2010). The QEPAS-based trace gas sensor is capable of ultra-sensitive trace gas detection and is suitable for real time breath measurements, due to the fast gas exchange inside a compact (<4 $cm^3$) QEPAS gas cell, which acts as an absorption detection module (ADM) or spectrophone.

The $NH_3$ breath sensor employs a CW, RT, DFB-QCL in a HHL package from Hamamatsu (www.hamamatsu.com). The RT operated DFB-QCL uses only air cooling, produced by a small electronics fan and a heatsink attached to the back of the laser. A 4 mm diameter ZnSe aspheric lens, with a working distance of 0.65 mm and clear aperture of 3.6 mm, was used to collimate the laser beam. The laser optical power, after being transmitted through the spectrophone was found to be 22 mW, which is ~90% of the initial power of the DFB-QCL operated at 17.5°C. The photoacoustic signal is detected by the QTF and is amplified by a low-noise transimpedance preamplifier and delivered to a control electronics unit (CEU) for further data

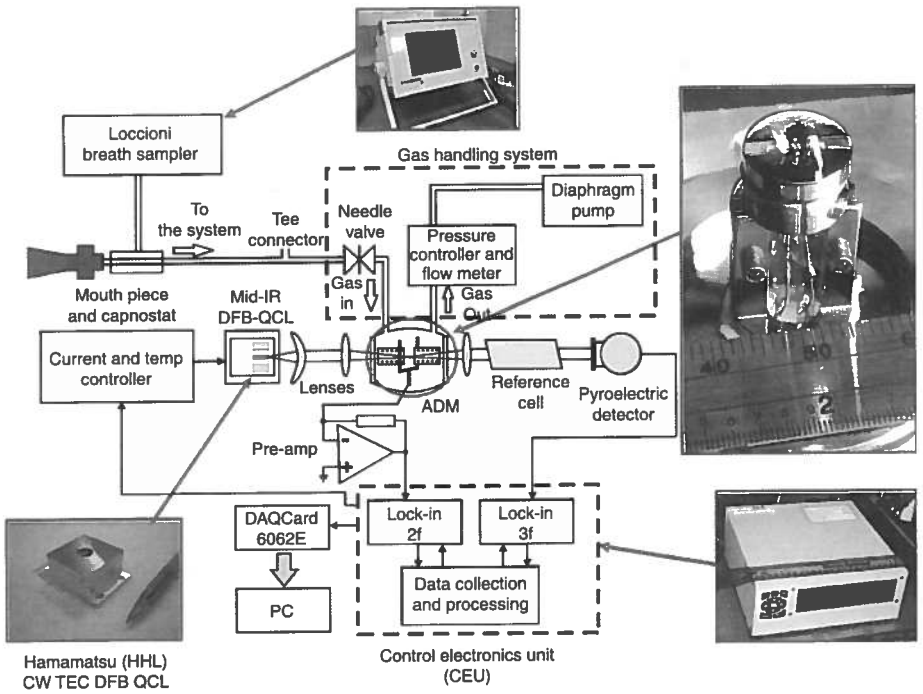


*15.10* Block diagram of $NH_3$ breath sensor architecture.

processing. A 10 cm long reference cell, filled with 0.2 % of $NH_3$ in $N_2$ at 130 Torr, and a pyroelectric detector were installed after the ADM module to lock the laser frequency to the center of the selected $NH_3$ absorption line. In addition, the $NH_3$ sensor employs a commercially available breath sampler (Loccioni, Italy) in order to monitor and maintain the pressure of the exhaled breath within an acceptable range and to measure the associated breath $CO_2$ concentration level. After a subject breathes into a mouth piece, the collected breath gas sample simultaneously enters the Loccioni breath sampler and the optical breath sensor. The flow rate through the $NH_3$ sensor was fixed by means of a needle valve to 220 ml/min and the pressure value was set and controlled at 130 Torr. In addition, the ADM, needle valve, and the mouth piece together with the Loccioni breath sampler pipe line were heated to $\geq 38^{\circ}C$ to avoid $NH_3$ adsorption on the various component surfaces of the sensor, as well as to prevent from condensation of the water vapor inside the $NH_3$ sensor.

The Hamamatsu CW RT DFB-QCL was designed to emit radiation at a wavelength of 10.34 μm, within the $\nu_2$ fundamental absorption band of ammonia. Within the available DFB-QCL tuning range (Fig. 15.11a) two potential $NH_3$ absorption lines of the similar intensity, which are free from $H_2O$, $CO_2$ and methanol interferences, can be targeted at 967.35 $cm^{-1}$ (10.34 μm) and 965.35 $cm^{-1}$ (10.36 μm). For QEPAS-based $NH_3$ measurements,

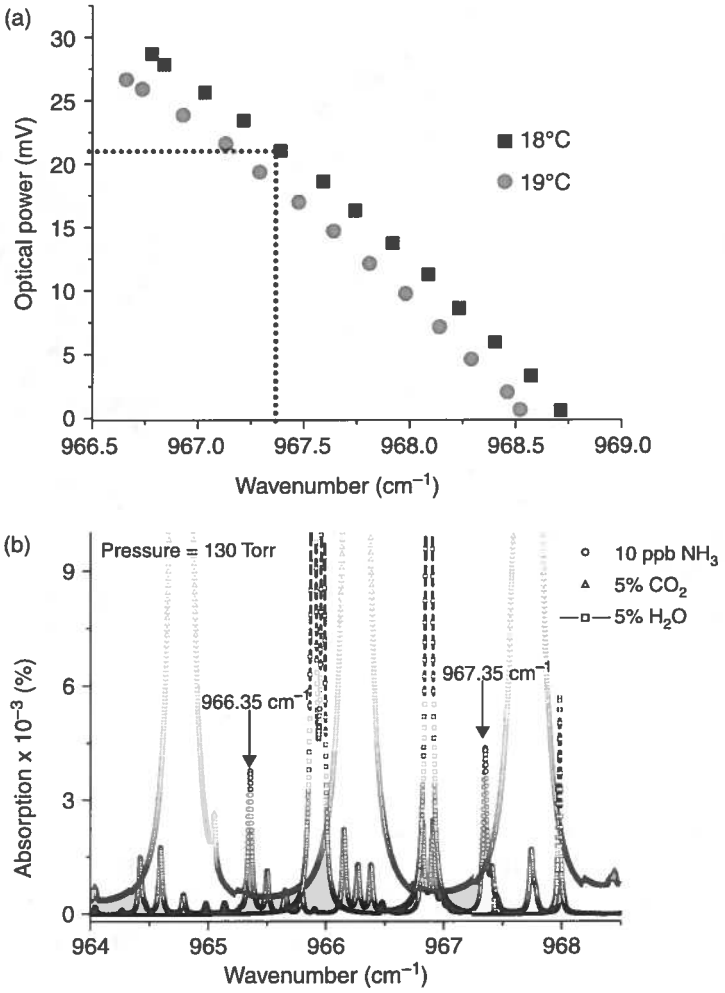


*15.11* (a) Optical power and current tuning of the CW DFB-QCL operated at two different quasi-RTs Laser power at targeted $NH_3$ line (967.35 cm$^{-1}$) is ~21mW. (b) HITRAN simulated spectra at 130 Torr indicating two potential $NH_3$ absorption lines of interest for exhaled breath measurements.

where the detected signal scales linearly with optical power, the absorption line located at 967.35 cm$^{-1}$ was the optimum selection due to a higher laser power compared to the power at 965.35 cm$^{-1}$. The HITRAN simulated spectra at 130 Torr, indicating $NH_3$ absorption lines together with the $CO_2$ and $H_2O$ absorption lines in the ~966 cm$^{-1}$ (10.35 μm) spectral region, are illustrated in Fig. 15.11b. Experimental data showed that for a 2f WM QEPAS scan performed within the spectral range of interest no overlap between 967.35 cm$^{-1}$ $NH_3$ and the adjacent $CO_2$ absorption line centered at 967.71 cm$^{-1}$ is present (Lewicki *et al.*, 2011). For a 2f WM QEPAS measurement,

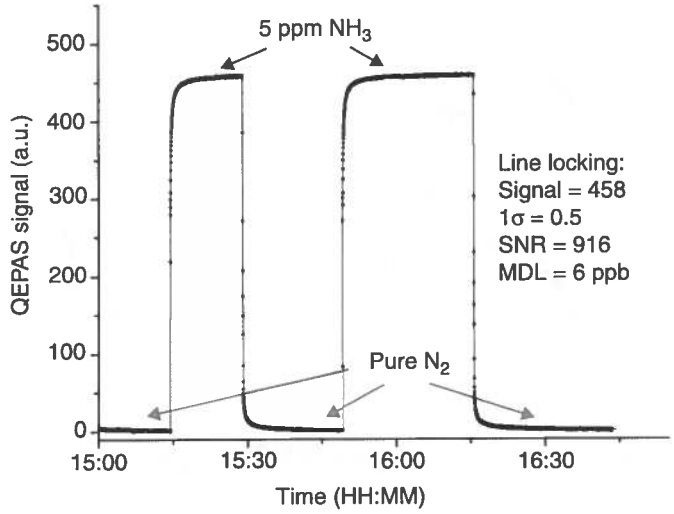


*15.12* 2f WM QEPAS signal when QCL was locked to the 967.35 $cm^{-1}$ (10.34 μm) $NH_3$ line. P = 130 Torr.

a 1σ minimum detectable concentration of ammonia was achieved at ~8 ppb when the laser frequency was current tuned over the 967.35 $cm^{-1}$ $NH_3$ absorption line. After locking the laser frequency to the 967.35 $cm^{-1}$ line, a 1σ minimum detectable $NH_3$ concentration was achieved of ~6 ppb with a 1 s time resolution (see Fig. 15.12).

A similar detection limit of ~5.4 ppb (1σ) was obtained after diluting a calibrated mixture of 5 ppm $NH_3$ in $N_2$ to a level of ~160 ppb (Lewicki *et al.*, 2011). This confirms the linear response of the QEPAS-based $NH_3$ sensor platform.

The $NH_3$ sensor system for the real time monitoring of ammonia concentration levels in exhaled breath was designed to collect breath samples multiple times with ~3 min intervals between each sample. These intervals are needed to remove the remaining ammonia out of the system. Examples of single breath exhalation profiles for $NH_3$ concentration (ppb), $CO_2$ concentration (%), and airway pressure (mbar) are depicted in Fig. 15.13. No significant delay between airway pressure and breath ammonia profile is observed, which confirms that the $NH_3$ sensor has an extremely fast response (<3 s). In addition, after the breath sampling process is completed, a fast ammonia decay from the system is also observed.

The $NH_3$ sensor is currently installed at a medical breath research center in Hellertown, PA, and is being evaluated as an instrument for non-invasive verification of liver and kidney disorders based on human breath samples. Real time exhaled human ammonia breath data, acquired in the medical breath research center, will be compared with simultaneously clinically acquired ammonia blood data.

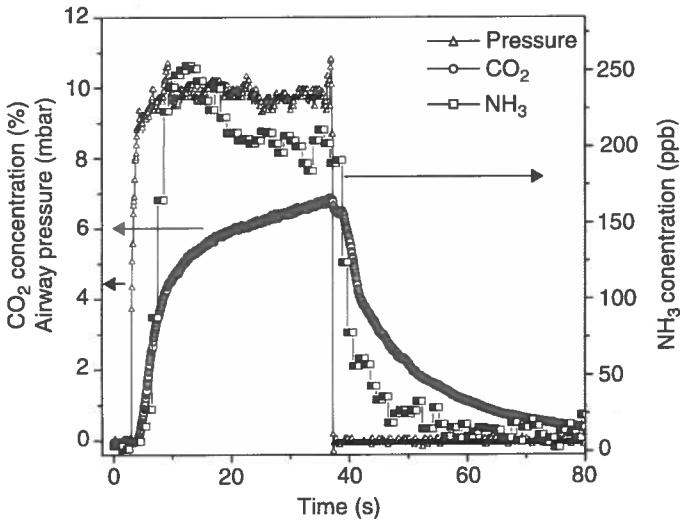


*15.13* $NH_3$ concentration, $CO_2$ concentration , and airway pressure profiles of a single breath exhalation.

## 15.4.3 Ammonia sensor for environmental monitoring based on a 10.3 μm EC-QCL

Ammonia ($NH_3$) is normally present in the atmosphere at trace concentration levels, and like other nitrogen-containing trace gases, such as $N_2O$, NO, $NO_2$, and $HNO_2$ or $HNO_3$, plays a significant role in atmospheric chemistry. The largest emission of $NH_3$ to the atmosphere is caused by anthropogenic sources such as animal waste, poultry, mineral fertilizers, agricultural crops, or biomass burning. Other significant sources of ammonia emission are natural sources such as animals, oceans, vegetation, and the decomposition of plants (Dentener and Crutzen, 1994). Moreover, for highly developed urban areas, an additional increase of atmospheric ammonia may be observed as the result of industrial activities and motor vehicles (Kean *et al.*, 2000). From an environmental perspective, $NH_3$ is a precursor of particulate matter, due to its chemical reaction with sulfuric and nitric acids to produce different ammonium salts such as ammonium sulfate ($(NH_4)_2SO_4$), ammonium nitrate ($NH_4NO_3$), and ammonium bisulfate ($NH_4HSO_4$). Generally, for rural areas, a main source of ammonia is cattle and other livestock, whereas in most of urban areas, other sources are dominant, such as industrial and traffic emissions (Russell *et al.*, 2004). The atmospheric concentrations of $NH_3$ for urban areas may vary between 0.1 and 10 ppbv, depending on the proximity to the source (Seinfeld and Pandis, 1998).

Therefore, to improve our understanding of the dynamics of $NH_3$ in industrial and urban area such as the Greater Houston area, where atmospheric

$NH_3$ data are limited, an EC-QCL-based ammonia sensor platform was deployed on the roof of the 60 m high North Moody Tower. The Moody Tower location (University of Houston, TX) was a perfect sampling site due to its proximity to many potential $NH_3$ emission sources such as the Houston Ship Channel and several highways (I-610, US 59, I-45). In addition, atmospheric $NH_3$ data were compared with data acquired by other advanced gas sensing instruments that were also installed at the Moody Tower air-quality monitoring site. This is useful for the determination of the implications of $NH_3$ with respect to atmospheric chemistry and air quality in Houston.

Determination of environmental ammonia concentration levels was performed with a 10.4 μm EC-QCL-based sensor platform (Fig. 15.14a). A CW TEC EC-QCL system from Daylight Solutions (Model 21106-MHF), emitting a maximum optical power of 72 mW within total tuning range from 933 $cm^{-1}$ to 1006 $cm^{-1}$, was implemented. As a detection technique, an amplitude modulated photoacoustic spectroscopy (AM-PAS) employing a ring differential resonant photoacoustic cell was used (Lee *et al.*, 2007). The differential cell with two cylindrical channels (each 6 mm diameter and 90 mm long) has an electret microphone placed in the middle, at a distance of 4 mm from the axis. A collimated laser beam (3 mm diameter) propagating through only one of the channels, was modulated by a mechanical chopper at 1.8 kHz in order to match the resonance frequency of the photoacoustic (PA) cell. To achieve $NH_3$ detection at single ppbv concentration levels, which is required for sensitive atmospheric measurements, the optical beam was passed through the cell three times (Fig. 15.14a). A pyroelectric detector placed after a 10-cm reference cell, which was filled with 0.2% of $NH_3$ at 30 Torr, is used for frequency locking EC-QCL wavelength to the selected optimum $NH_3$ absorption line as well as for monitoring the EC-QCL power

The pressure inside the sensor system was kept at 220 Torr and the flow was maintained at 150 ml/min. In order to minimize the ammonia adsorption to surfaces and to prevent water vapor condensation in the sensor, the sensor enclosure was heated to +38°C. Moreover, a pump maintained a high flow of ~10 l/s between sampling port and the $NH_3$ sensor inlet in order to ensure laminar flow inside the tubing and to improve the $NH_3$ sensor response time to <2 min. The 965.35 $cm^{-1}$ (see Fig. 15.11b) absorption line in the $\nu_2$ fundamental absorption band of $NH_3$ was targeted for the monitoring of environmental $NH_3$ at trace gas concentration levels. Upon consideration of laser power, $NH_3$ absorption strength, and potential interferences from $H_2O$, $CO_2$, and methanol ($CH_3OH$) molecules, this frequency was the optimum selection for the AM-PAS technique.

For high-resolution $NH_3$ measurements with the AM-PAS technique, an EC-QCL MHF tuning range of 0.15 $cm^{-1}$ was selected to cover only the $NH_3$ absorption line of interest. The $NH_3$ measurements for the detection of

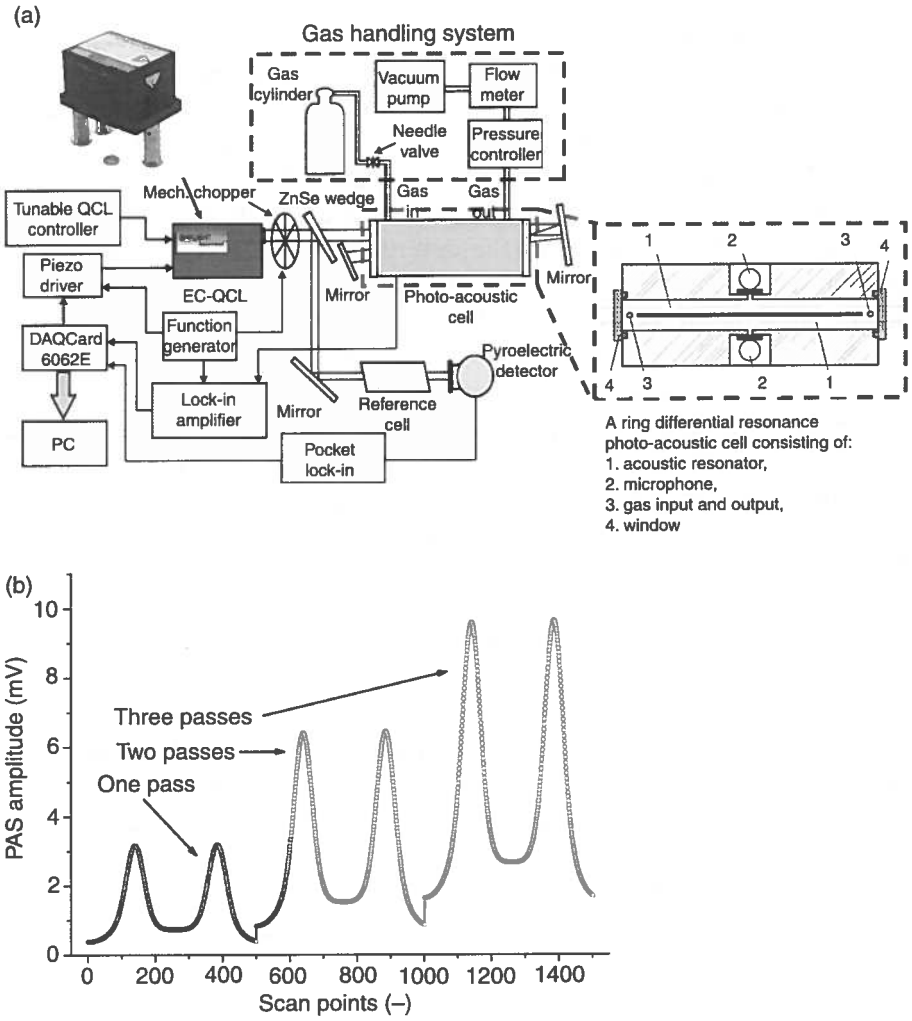


*15.14* (a) Mid-infrared AM-PAS-based sensor platform for atmospheric $NH_3$ detection; (b) AM-PAS signal for a reference mixture of 5 ppmv $NH_3$ in $N_2$ after one, two, and three QCL output beam passes through the photoacoustic cell. 5 ppmv of $NH_3$ in $N_2$ at 220 Torr; $NH_3$ line at 985.35 $cm^{-1}$; MDL ~2 ppbv.

ammonia concentration levels were performed using a scan mode, where the EC-QCL wavelength was scanned back and forth across the 965.35 $cm^{-1}$ $NH_3$ line, with a frequency of $f = 0.2$ Hz. In this case a profile of the $NH_3$ absorption line was detected twice in order to improve the accuracy of the $NH_3$ concentration calculation procedure. The minimum detectable concentration of ammonia for the laboratory tested sensor, when the laser beam passes three times through the PA cell, was ~2 ppbv for a 5-second data acquisition time (Fig. 15.14b). By monitoring the peak position of the $NH_3$ absorption line

profile recorded by the pyroelectric detector, any potential EC-QCL wavelength drift can be identified and used for laser frequency stabilization. Thus, any rising laser drift was eliminated by sending a PID correction signal to the EC-QCL piezo element which is responsible for wavelength tuning.

In order to calibrate the $NH_3$ sensor, a LabView-based, general least-square (LS) linear fitting algorithm was implemented to determine the best correlation between each acquired sample scan and the 5 ppmv $NH_3$ reference scan. For each scan the concentration levels (expressed in unit of parts-per-billion) of atmospheric ammonia were calculated based on a fit coefficient, which was found and returned by the LS linear fitting procedure. For the sample scan data that perfectly coincides with a reference scan data, the linear fit coefficient will be equal to unity, which implies that the measured ammonia concentration is identical with reference concentration. The benefit of using scan mode and the linear fitting procedure is its insensitivity to potential baseline drifts or background variations, which are typically observed for AM-based spectroscopic measurements. Therefore, by using a direct comparison of measured and reference scans, an exact evaluation of the gas concentration was achieved. An alternative to the AM detection scheme would be a background-free 2f WM scheme. However, the frequency range acceptable for the EC-QCL for current modulation is limited to frequencies between 10 kHz and 2 MHz. This frequency range is too high to perform WM-based spectroscopic measurements that employs a PA cell that possesses an internal resonance frequency of ~1.8 kHz.

The AM-PAS-based sensor platform was deployed on the roof of the Moody Tower building (University of Houston campus) to monitor atmospheric ammonia concentration levels between a two-week period in February 2010, a two-month period over the course of August to October 2010, and a two-week period during February 2011. To investigate the long-term stability of the ammonia sensor system, a set of data was acquired while pure nitrogen was flushed through the sensor PA cell and an Allan variance analysis was performed. The EC-QCL-based $NH_3$ sensor platform (see Fig. 15.14a), after its installation at the Moody Tower site, demonstrated an MDL for ammonia concentration at the ~ 3.4 ppbv level with a 5-second data acquisition time. After averaging the $NH_3$ concentration data for ~300 s, a sub-ppbv $NH_3$ concentration level of ~0.72 ppbv was achieved. For the purpose of environmental monitoring, where sensor time response is not a critical parameter, even longer averaging times can be utilized to allow a sub-ppb detection limit of $NH_3$.

A time series of atmospheric $NH_3$ concentration levels (after 300-seconds averaging time), measured during the 2010 summer/fall season, was demonstrated in Fig. 15.15. Within the two months of the $NH_3$ sensor deployment at Moody Tower, several unexpected events of high $NH_3$ concentrations levels were observed. The emission sources of a several long lasting $NH_3$

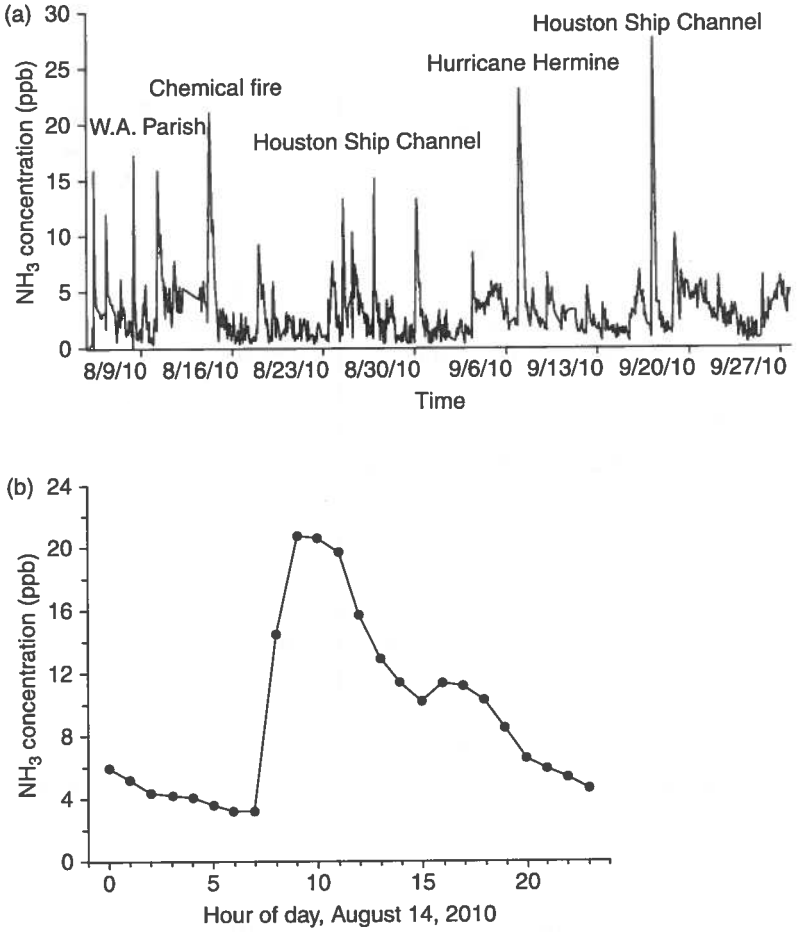


*15.15* (a) A time series of $NH_3$ concentrations measured during summer/fall 2010. (b) Accidental ammonia release from a chemical fire resulting from a collision of 18-wheeler trucks on the Houston-Gulf Freeway (I-45) only 2 miles from the sampling site.

concentration peaks were determined by monitoring wind direction and employing backward trajectory analysis in order to check the air mass transport path. The emission sources that were identified as being responsible for increased $NH_3$ concentration levels in the Greater Houston urban area are: the Houston Ship Channel, W. A. Parish electric power plant, the ocean (Hurricane Hermine), and traffic activity including a traffic accident that caused a chemical fire on I-45 freeway.

The dominant $NH_3$ source for the Greater Houston area was found to be related to industrial and petrochemical activity around the Houston Ship Channel. This is not surprising, because hourly estimated $NH_3$ emission into the atmosphere from the Houston Ship Channel area is estimated to

be ~120 kg (Mellqvist *et al.*, 2007). The $NH_3$ emission from the W. A. Parish power plant located 27 miles SE of Moody Tower also strongly contributed to the atmospheric $NH_3$ concentration level. This is because the selective catalytic reduction process in the power plant employs ammonia gas as a reactant to reduce NOx emissions by converting it into nitrogen gas and water. During this process $NH_3$ is released into the atmosphere when the temperature levels of the chemical reaction are not properly maintained or when too much ammonia is injected into the system. An unexpected increase of the $NH_3$ concentration (~21 ppb) on August 14, 2010 was observed (see Fig. 15.15b), when a major accident occurred during the same time period on the Houston-Gulf Freeway (I-45), two miles from the sampling site. The elevated concentration levels are due to $NH_3$ generation from a chemical fire resulting from a collision of two 18-wheeler trucks, one of which was carrying a fertilizer (trimethylammonium) and liquid pesticide (dimethylamine).

## 15.5 Conclusions and future trends

Spectroscopic techniques that include Compact, reliable, real time, sensitive ($<10^{-4}$), and highly selective (<3 to 500 MHz) gas sensors based on QCL-based LAS, CRDS, ICOS, CPAS and QEPAS, evanescent wave spectroscopy, laser-induced breakdown spectroscopy (LIBS), noise-immune cavity-enhanced optical heterodyne molecular spectroscopy (NICE-OHMS), cavity-enhanced optical frequency comb spectroscopy (CE-FCS) have become important as scientific and industrial techniques. LAS has benefited significantly from the development of infrared laser sources that can access the desired mid-infrared wavelengths, novel measurement techniques and improved data acquisition and reduction methods. The choice of a specific spectroscopic measurement method is determined by the application as well as the readily commercial availability of QCLs with powers of >100 mW and operating lifetimes comparable to near-infrared laser diodes (~10 years). Furthermore, improvements and innovations in LAS, CRDS, ICOS and QEPAS sensor platforms – in particular, more stable, mass produced optical/mechanical designs – as well as data acquisition and reduction techniques, will lead to mid-infrared QCL- and ICL-based instruments that can be operated by non-technical personnel and be manufactured at costs leading to sensor networks that permit both temporal and spatial trace gas monitoring. Autonomously operated compact, reliable, real time, sensitive ($<10^{-4}$), and highly selective (<3 to 500 MHz) gas sensors based on various spectroscopic techniques using QCLs and ICLs have been demonstrated to be effective in numerous real world and fundamental science applications. These include such diverse fields as atmospheric chemistry and environmental monitoring (e.g., CO, $CO_2$, $CH_4$ and $H_2CO$ are important carbon gases in global warming), ozone depletion studies, acid rain, photo smog formation),

industrial emission measurements (e.g., quantification of smokestack emissions, fence line perimeter monitoring by the petrochemical industry, combustion incinerators, down hole gas monitoring, gas pipeline and industrial plant safety), urban (e.g., automobile, truck, aircraft, marine and electrical power generation) and rural emissions (e.g., horticultural greenhouses, fruit storage and rice agro-ecosystems). Furthermore sensors are used in chemical analysis and process control for manufacturing processes (e.g., petrochemical processing and exploration, alternative energy technologies and production, semiconductor wafer manufacture, pharmaceutical, metal processing, nuclear safeguards, food and beverage industries), applications in biomedical and the life sciences, such as non-invasive medical diagnostics that involves the detection and monitoring of numerous exhaled breath biomarkers (e.g., NO, CO, $CO_2$, $NH_3$, $C_2H_6$ and $CH_3COCH_3$). In addition, EC-QCL-and DFB-QCL-based spectroscopic methods and instruments for sensing of toxic gases and explosives relevant to law enforcement, national security and defense (Willer and Schade, 2009; Bauer *et al.*, 2010; Holthoff *et al.*, 2010), as well as spacecraft habitat air quality and safety (e.g., outgassing of $H_2CO$ from industrial components, fire and post fire detection) and planetary atmospheric science (e.g., planetary gases such as $H_2O$, $CH_4$, CO, $CO_2$ and $C_2H_2$). With the development of efficient mid-infrared lasers (Curl *et al.*, 2010; Bewley *et al.*, 2010; Troccoli *et al.*, 2010; Razeghi *et al.*, 2010; Lyakh *et al.*, 2010) we envision a significantly improved performance coupled with a reduction in size and cost of thermoelectrically cooled QCL-and ICL-based trace gas monitors that will lead to the implementation of sensor networks (So *et al.*, 2009, 2010). Sensor networks based on LAS and QEPAS will enable large-area detection of trace gas fluxes, mapping and localization of emission sources, as well as the identification of unknown natural gas sinks.

## 15.6 References

Adams, H., Reinert, D., Kalkert, P. and Urban, W. (1984) 'A differential detection scheme for Faraday rotation spectroscopy with a color center laser', *Appl. Phys. B*, **34**, 179–185.

Aellen, T., Blaser, S., Beck, M., Hofstetter, D., Faist, J. and Gini, E. (2003) 'Continuous-wave distributed-feedback quantum-cascade lasers on a Peltier cooler', *Appl. Phys. Lett.*, **83**, 1929–1931.

Arnold, A. S., Wilson, J. S. and Boshier, M. G. (1998) 'A simple extended-cavity diode laser', *Rev. Sci. Instrum.*, **69**, 1236–1239.

Bakhirkin, Y. A., Kosterev, A. A., Curl, R. F., Tittel, F. K., Yarekha, D. A., Hvozdara, L., Giovannini, M. and Faist, J. (2006) 'Sub-ppbv nitric oxide concentration measurements using cw thermoelectrically cooled quantum cascade laser-based integrated cavity output spectroscopy', *Appl. Phys. B*, **82**, 149–154.

Bakhirkin, Y. A., Kosterev, A. A., Roller, C., Curl, R. F. and Tittel, F. K. (2004) 'Mid-infrared quantum cascade laser based off-axis integrated cavity output spectroscopy for biogenic nitric oxide detection', *Appl. Opt.*, **43**, 2257–2266.

Bauer, C., Willer, U., Lewicki, R., Pohlkötter, A., Kosterev, A., Kosynkin, D., Tittel, F. K. and Schade, W. (2009) 'A Mid-infrared QEPAS sensor device for TATP detection', *Journal of Physics: Conference Series*, **157**, 012002.

Bauer, C., Willer, U. and Schade, W. (2010) 'Use of quantum cascade lasers for detection of explosives: progress and challenges', *Opt. Eng.*, **49**, 111126.

Belenky, G., Shterengas, L., Kipshidze, G. and Hosoda, T. (2011) 'Type-I diode lasers for spectral region above 3 mm', *IEEE J. Sel. Topics in Quantum Electron.*, **17**, 1426–1434.

Bernegger, S. and Sigrist, M. W. (1990) 'CO-laser photoacoustic spectroscopy of gases and vapours for trace gas analysis', *Infrared Phys.*, **30**, 375–429.

Bewley, W., Canedy, C., Kim, C. S., Kim, M., Lindle, J. R., Abell, J., Vurgaftman, I. and Meyer, J. (2010) 'Ridge-width dependence of midinfrared interband cascade laser characteristics', *Opt. Eng.*, **49**, 111116.

Bijnen, F. G. C., Reuss, J. and Harren, F. J. M. (1996) 'Geometrical optimization of a longitudinal resonant photoacoustic cell for sensitive and fast trace gas detection', *Rev. Sci. Instrum.*, **67**, 2914–2923.

Bismuto, A., Beck, M. and Faist, J. (2011) 'High power Sb-free quantum cascade laser emitting at 3.3 mm above 350 K', *Appl. Physics Lett.*, **98**, 191104.

Brecha, R. J., Pedrotti, L. M. and Krause, D. (1997) 'Magnetic rotation spectroscopy of molecular oxygen with a diode laser', *J. Opt. Soc. Am. B*, **14**, 1921–1930.

Busch, W. K. and Busch, A. M. (1999) 'Introduction to cavity-ringdown spectroscopy'. In *Cavity-Ringdown Spectroscopy*, American Chemical Society, pp. 7–19.

Caffey, D., Day, T., Kim, C. S., Kim, M., Vurgaftman, I., Bewley, W. W., Lindle, J. R., Canedy, C. L., Abell, J. and Meyer, J. R. (2010) 'Performance characteristics of a continuous-wave compact widely tunable external cavity interband cascade lasers', *Opt. Express*, **18**, 15691–15696.

Capasso, F. (2010) 'High-performance midinfrared quantum cascade lasers', *Opt. Eng.*, **49**, 111102.

Cheng, W.-H. and Lee, W.-J. (1999) 'Technology development in breath microanalysis for clinical diagnosis', *J. Lab. Clin. Med.*, **133**, 218–228.

Christensen, L. E., Mansour, K. and Yang, R. Q. (2010) 'Thermoelectrically cooled interband cascade laser for field measurements', *Opt. Eng.*, **49**, 111119.

Costopoulos, D., Miklós, A. and Hess, P. (2002) 'Detection of $N_2O$ by photoacoustic spectroscopy with a compact, pulsed optical parametric oscillator', *Appl. Phys. B: Lasers and Optics*, **75**, 385–389.

Curl, R. F., Capasso, F., Gmachl, C., Kosterev, A. A., McManus, B., Lewicki, R., Pusharsky, M., Wysocki, G. and Tittel, F. K. (2010) 'Quantum cascade lasers in chemical physics', *Chem. Phys. Lett.*, **487**, 1–18.

da Silva, M. G., Vargas, H., Miklós, A. and Hess, P. (2004) 'Photoacoustic detection of ozone using a quantum cascade laser', *Appl. Phys. B: Lasers and Optics*, **78**, 677–680.

Day, T. (2010) External cavity quantum cascade lasers: recent advances, applications, comparisons with alternative sources in the MIR. In *Laser Applications to Chemical, Security and Environmental Analysis*, San Diego, California, Optical Society of America, JTuA1.

Day, T., Arnone, D., Crivello, S. F. and Weida, M. J. (2006) Miniaturized external cavity quantum cascade lasers for broad tunability in the mid-infrared, translated by 1–2.

Dentener, F. J. and Crutzen, P. J. (1994) 'A three-dimensional model of the global ammonia cycle', *J. Atmos. Chem.*, **19**, 331–369.

Dillenschneider, W. and Curl, R. F. (1983) 'Color center laser spectroscopy of n1 + n2 + n3 of $NO_2$ using magnetic rotation', *J. Mol. Spectrosc.*, **99**, 87–97.

Dong, L., Kosterev, A., Thomazy, D. and Tittel, F. (2010) 'QEPAS spectrophones: design, optimization, and performance', *Appl. Phys. B: Lasers and Optics*, **100**, 627–635.

Dweik, R. A. and Amann, A. (2008) 'Exhaled breath analysis: the new frontier in medical testing', *J. Breath Res.*, **2**, 030301.

Elia, A., Lugarà, P. M., Di Franco, C. and Spagnolo, V. (2009) 'Photoacoustic techniques for trace gas sensing based on semiconductor laser sources', *Sensors*, **9**, 9616–9628.

Elia, A., Lugarà, P. M. and Giancaspro, C. (2005) 'Photoacoustic detection of nitric oxide by use of a quantum-cascade laser', *Opt. Lett.*, **30**, 988–990.

Engel, G. S., Drisdell, W. S., Keutsch, F. N., Moyer, E. J. and Anderson, J. G. (2006) 'Ultrasensitive near-infrared integrated cavity output spectroscopy technique for detection of CO at 1.57 μm: new sensitivity limits for absorption measurements in passive optical cavities', *Appl. Opt.*, **45**, 9221–9229.

Faist, J., Beck, M., Aellen, T. and Gini, E. (2001) 'Quantum-cascade lasers based on a bound-to-continuum transition', *Appl. Phys. Lett.*, **78**, 147–149.

Faist, J., Capasso, F., Sivco, D. L., Hutchinson, A. L. and Cho, A. Y. (1994) 'Quantum cascade laser', *Science*, **264**, 553–556.

Faist, J., Gmachl, C., Capasso, F., Sitori, C., Sivco, D. L., Baillargeon, J. N., Hutchinson, A. L. and Cho, A. Y. (1997) 'Distributed feedback quantum cascade lasers', *Appl. Phys. Lett.*, **70**, 2670–2672.

Faist, J., Hofstetter, D., Beck, M., Aellen, T., Rochat, M. and Blaser, S. (2002) 'Bound-to-continuum and two-phonon resonance quantum-cascade lasers for high duty cycle, high-temperature operation', *IEEE J. Quantum Electron.*, **38**, 533–546.

Foltynowicz, A., Schmidt, F. M., Ma, W. and Axner, O. (2008) 'Noise-immune cavity-enhanced optical heterodyne molecular spectroscopy: Current status and future potential', *Appl. Phys. B: Lasers and Optics*, **92**, 313–326.

Fried, A., Henry, B., Wert, B., Sewell, S. and Drummond, J. R. (1998) 'Laboratory, ground-based, and airborne tunable diode laser systems: performance characteristics and applications in atmospheric studies', *App. Phys. B: Lasers and Optics*, **67**, 317–330.

Fried, A. and Richter, D. (2007) 'Infrared absorption spectroscopy'. In *Analytical Techniques for Atmospheric Measurement*, Blackwell Publishing, pp. 72–146.

Fried, A., Sewell, S., Henry, B., Wert, B. P., Gilpin, T. and Drummond, J. R. (1997) 'Tunable diode laser absorption spectrometer for ground-based measurements of formaldehyde', *J. Geophys. Res.*, **102**(D5), 6253–6266.

Fritsch, T., Horstjann, M., Halmer, D., Sabana, Hering, P. and Mürtz, M. (2008) 'Magnetic Faraday modulation spectroscopy of the 1–0 band of $^{14}NO$ and $^{15}NO$', *Appl. Phys. B: Lasers and Optics,* **93**, 713–723.

Fujita, K., Edamura, T., Furuta, S. and Yamanishi, M. (2010) 'High-performance, homogeneous broad-gain quantum cascade lasers based on dual-upper-state design', *Appl. Phys. Lett.*, **96**, 241107.

Ganser, H., Horstjann, M., Suschek, C. V., Hering, P. and Mürtz, M. (2004) 'Online monitoring of biogenic nitric oxide with a QC laser-based Faraday modulation technique', *Appl. Phys. B: Lasers and Optics*, **78**, 513–517.

Ganser, H., Urban, W. and Brown, A. M. (2003) 'The sensitive detection of NO by Faraday modulation spectroscopy with a quantum cascade laser', *Molec. Phys.*, **101**, 545–550.

Gmachl, C., Capasso, F., Faist, J., Hutchinson, A. L., Tredicucci, A., Sivco, D. L., Baillargeon, J. N., Chu, S. N. G. and Cho, A. Y. (1998) 'Continuous-wave and high-power pulsed operation of index-coupled distributed feedback quantum cascade laser at l≈ 8.5 μm', *Appl. Phys. Lett.*, **72**, 1430–1432.

Gmachl, C., Sivco, D. L., Baillargeon, J. N., Hutchinson, A. L., Capasso, F. and Cho, A. Y. (2001) 'Quantum cascade lasers with a heterogeneous cascade: Two-wavelength operation', *Appl. Phys. Lett.*, **79**, 572–574.

Gmachl, C., Sivco, D. L., Colombelli, R., Capasso, F. and Cho, A. Y. (2002) 'Ultra-broadband semiconductor laser', *Nature*, **415**, 883–887.

Gottfried, J., De Lucia, F., Munson, C. and Miziolek, A. (2009) 'Laser-induced breakdown spectroscopy for detection of explosives residues: a review of recent advances, challenges, and future prospects', *Anal. Bioanal. Chem.*, **395**, 283–300.

Grober, R. D., Acimovic, J., Schuck, J., Hessman, D., Kindlemann, P. J., Hespanha, J., Morse, A. S., Karrai, K., Tiemann, I. and Manus, S. (2000) 'Fundamental limits to force detection using quartz tuning forks', *Rev. Sci. Instrum.*, **71**, 2776–2780.

Grossel, A., Zéninari, V., Parvitte, B., Joly, L., Courtois, D. and Durry, G. (2008) 'Quantum cascade laser spectroscopy of $N_2O$ in the 7.9 μm region for the in situ monitoring of the atmosphere', *J. Quant. Spectrosc. Radiat. Transfer*, **109**, 1845–1855.

Guipeng, L., Chuan, P., Le, H. Q., Shin-Shem, P., Hao, L., Wen-Yen, H., Ishaug, B. and Jun, Z. (2002) 'Broadly wavelength-tunable external cavity, mid-infrared quantum cascade lasers', *IEEE J. Quantum Electron.*, **38**, 486–494.

Gupta, J. A., Ventrudo, B. F., Waldron, P. and Barrios, P. J. (2010) 'External cavity tunable type-I diode laser with continuous-wave singlemode operation at 3.24 μm', *Electron. Lett.*, **46**, 1218–1220.

Hofstetter, D., Beck, M., Aellen, T. and Faist, J. (2001a) 'High-temperature operation of distributed feedback quantum-cascade lasers at 5.3 μm', *Appl. Phys. Lett.*, **78**, 396.

Hofstetter, D., Beck, M., Faist, J., Nägele, M. and Sigrist, M. W. (2001b) 'Photoacoustic spectroscopy with quantum cascade distributed-feedback lasers', *Opt. Lett.*, **26**, 887–889.

Hofstetter, D., Faist, J., Beck, M., Muller, A. and Oesterle, U. (1999) 'Demonstration of high-performance 10.16 μm quantum cascade distributed feedback lasers fabricated without epitaxial regrowth', *Appl. Phys. Lett.*, **75**, 665–667.

Holthoff, E. L., Heaps, D. A. and Pellegrino, P. M. (2010) 'Development of a MEMS-scale photoacoustic chemical sensor using a quantum cascade laser', *Sensors J., IEEE*, **10**, 572–577.

Horstjann, M., Bakhirkin, Y. A., Kosterev, A. A., Curl, R. F., Tittel, F. K., Wong, C. M., Hill, C. J. and Yang, R. Q. (2004) 'Formaldehyde sensor using interband cascade laser based quartz-enhanced photoacoustic spectroscopy', *Appl. Phys. B*, **79**, 799–803.

Hugi, A., Maulini, R. and Faist, J. (2010) 'External cavity quantum cascade laser', *Semiconductor Sci. Technol.*, **25**, 083001.

Hugi, A., Terazzi, R., Bonetti, Y., Wittmann *et al.*, A., Fischer, M., Beck, M., Faist, J. and Gini, E. (2009) 'External cavity quantum cascade laser tunable from 7.6 to 11.4 μm', *Appl. Phys. Lett.*, **95**, 061103.

Karpf, A. and Rao, G. N. (2009) 'Absorption and wavelength modulation spectroscopy of $NO_2$ using a tunable, external cavity continuous wave quantum cascade laser', *Appl. Opt.*, **48**, 408–413.

Kean, A. J., Harley, R. A., Littlejohn, D. and Kendall, G. R. (2000) 'On-road measurement of ammonia and other motor vehicle exhaust emissions', *Environ. Sci. Technol.*, **34**, 3535–3539.

Kluczynski, P., Lundqvist, S., Westberg, J. and Axner, O. (2011) 'Faraday rotation spectrometer with sub-second response time for detection of nitric oxide using a cw DFB quantum cascade laser at 5.33 μm', *Appl. Phys. B: Lasers and Optics*, **103**, 451–459.

Kneepkens, F., Lepage, G. and Roy, C. C. (1994) 'The potential of the hydrocarbon breath test as a measure of lipid peroxidation', *Free Radical Biol. Med.*, **17**, 127–160.

Köhring, M., Pohlkötter, A., Willer, U., Angelmahr, M. and Schade, W. (2011) 'Tuning fork enhanced interferometric photoacoustic spectroscopy: a new method for trace gas analysis', *Appl. Phys. B: Lasers and Optics*, **102**, 133–139.

Kosterev, A. A., Bakhirkin, Y. A., Curl, R. F. and Tittel, F. K. (2002) 'Quartz-enhanced photoacoustic spectroscopy', *Opt. Lett.*, **27**, 1902–1904.

Kosterev, A. A., Bakhirkin, Y. A. and Tittel, F. K. (2005a) 'Ultrasensitive gas detection by quartz-enhanced photoacoustic spectroscopy in the fundamental molecular absorption bands region', *Appl. Phys. B*, **80**, 133–138.

Kosterev, A. A., Bakhirkin, Y. A., Tittel, F. K., Blaser, S., Bonetti, Y. and Hvozdara, L. (2004) 'Photoacoustic phase shift as a chemically selective spectroscopic parameter', *Appl. Phys. B*, **78**, 673–676.

Kosterev, A. A., Buerki, P., Dong, L., Reed, M., Day, T. and Tittel, F. (2010a) 'QEPAS detector for rapid spectral measurements', *Appl. Phys. B: Lasers and Optics*, **100**, 173–180.

Kosterev, A. A., Dong, L., Thomazy, D., Tittel, F. and Overby, S. (2010b) 'QEPAS for chemical analysis of multi-component gas mixtures', *Appl. Phys. B: Lasers and Optics*, **101**, 649–659.

Kosterev, A. A. and Doty, J. H. III (2010) 'Resonant optothermoacoustic detection: technique for measuring weak optical absorption by gases and micro-objects', *Opt. Lett.*, **35**, 3571–3573.

Kosterev, A. A., Malinovsky, A. L., Tittel, F. K., Gmachl, C., Capasso, F., Sivco, D. L., Baillargeon, J. N., Hutchinson, A. L. and Cho, A. Y. (2001) 'Cavity ringdown spectroscopic detection of nitric oxide with a continuous-wave quantum-cascade laser', *Appl. Opt.*, **40**, 5522–5529.

Kosterev, A. A., Mosely, T. S. and Tittel, F. K. (2006) 'Impact of humidity on quartz-enhanced photoacoustic spectroscopy based detection of HCN', *Appl. Phys. B: Lasers and Optics*, **85**, 295–300.

Kosterev, A. A. and Tittel, F. K. (2004) 'Ammonia detection by use of quartz-enhanced photoacoustic spectroscopy with a near-IR telecommunication diode laser', *Appl. Opt.*, **43**, 6213–6217.

Kosterev, A. A. and Tittel, F. K. (2002b) 'Chemical sensors based on quantum cascade lasers', *IEEE J. Quantum Electron.*, **38**, 582–591.

Kosterev, A. A., Tittel, F. K., Serebryakov, D. V., Malinovsky, A. L. and Morozov, I. V. (2005b) 'Applications of quartz tuning forks in spectroscopic gas sensing', *Rev. Sci. Instrum.*, **76**, 43105–43105.

Kosterev, A. A., Wysocki, G., Bakhirkin, Y., So, S., Lewicki, R., Fraser, M., Tittel, F. and Curl, R. F. (2008) 'Application of quantum cascade lasers to trace gas analysis', *Appl. Phys. B: Lasers and Optics*, **90**, 165–176.

Lee, B., Wood, E., Zahniser, M., McManus, J., Nelson, D., Herndon, S., Santoni, G., Wofsy, S. and Munger, J. (2011) 'Simultaneous measurements of atmospheric HONO and $NO_2$ via absorption spectroscopy using tunable mid-infrared continuous-wave quantum cascade lasers', *Appl. Phys. B: Lasers and Optics*, **102**, 417–423.

Lee, B. G., Belkin, M. A., Audet, R., MacArthur, J., Diehl, L., Pflugl, C. and Capasso, F. (2007) 'Widely tunable single-mode quantum cascade laser source for mid-infrared spectroscopy', *Appl. Phys. Lett.*, **91**, 231101.

Lee, B. G., Belkin, M. A., Pfugl, C., Diehl, L., Zhang, H. F. A., Audet, R. M., MacArthur, J., Bour, D. P., Corzine, S. W., Hofler, G. E. and Capasso, F. (2009a) 'DFB Quantum Cascade Laser Arrays', *IEEE J. Quantum Electron.*, **45**, 554–565.

Lee, B. G., Zhang, H. F. A., Pflugl, C., Diehl, L., Belkin, M. A., Fischer, M., Wittmann, A., Faist, J. and Capasso, F. (2009b) 'Broadband distributed-feedback quantum cascade laser array operating from 8.0 to 9.8 μm', *IEEE Photon. Technol. Lett.*, **21**, 914–916.

Lee, C.-M., Bychkov, K. V., Kapitanov, V. A., Karapuzikov, A. I., Ponomarev, Y. N., Sherstov, I. V. and Vasiliev, V. A. (2007) 'High-sensitivity laser photoacoustic leak detector', *Opt. Eng.*, **46**, 064302.

Lewicki, R., Doty, J. H., Curl, R. F., Tittel, F. K. and Wysocki, G. (2009) 'Ultrasensitive detection of nitric oxide at 5.33 μm by using external cavity quantum cascade laser-based Faraday rotation spectroscopy', *Proc. Natl Acad. Sci. USA*, **106**, 12587–12592.

Lewicki, R., Kosterev, A. A., Thomazy, D. M., Risby, T. H., Solga, S., Schwartz, T. B. and Tittel, F. K. (2011) 'Real time ammonia detection in exhaled human breath using a distributed feedback quantum cascade laser based sensor', *Proc. of SPIE 7945: 50K-2*.

Lewicki, R., Wysocki, G., Kosterev, A. A. and Tittel, F. K. (2007a) 'Carbon dioxide and ammonia detection using 2 μm diode laser based quartz-enhanced photoacoustic spectroscopy', *Appl. Phys. B: Lasers and Optics*, **87**, 157–162.

Lewicki, R., Wysocki, G., Kosterev, A. A. and Tittel, F. K. (2007b) 'QEPAS based detection of broadband absorbing molecules using a widely tunable, cw quantum cascade laser at 8.4 μm', *Opt. Express*, **15**, 7357–7366.

Lima, J. P., Vargas, H., Miklós, A., Angelmahr, M. and Hess, P. (2006) 'Photoacoustic detection of $NO_2$ and $N_2O$ using quantum cascade lasers', *Appl. Phys. B: Lasers and Optics*, **85**, 279–284.

Litfin, G., Pollock, C. R., Curl, R. F. and Tittel, F. K. (1980) 'Sensitivity enhancement of laser absorption spectroscopy by magnetic rotation effect', *J. Chem. Phys.*, **72**, 6602–6605.

Liu, K., Guo, X. Y., Yi, H. M., Chen, W. D., Zhang, W. J. and Gao, X. M. (2009) 'Off-beam quartz-enhanced photoacoustic spectroscopy', *Opt. Lett.*, **34**, 1594–1596.

Liu, K., Yi, H., Kosterev, A. A., Chen, W., Dong, L., Wang, L., Tan, T., Zhang, W., Tittel, F. K. and Gao, X. (2010) 'Trace gas detection based on off-beam quartz enhanced photoacoustic spectroscopy: Optimization and performance evaluation', *Rev. Sci. Instrum.*, **81**, 103103.

Lu, Q. Y., Bai, Y., Bandyopadhyay, N., Slivken, S. and Razeghi, M. (2011) '2.4 W room temperature continuous wave operation of distributed feedback quantum cascade lasers', *Appl. Phys. Lett.*, **98**, 181106.

Lyakh, A., Maulini, R., Tsekoun, A. G. and Patel, C. K. N. (2010) 'Progress in high-performance quantum cascade lasers', *Opt. Eng.*, **49**, 111105.

Manne, J., Sukhorukov, O., Jager, W. and Tulip, J. (2006) 'Pulsed quantum cascade laser-based cavity ring-down spectroscopy for ammonia detection in breath', *Appl. Opt.*, **45**, 9230–9237.

Maulini, R., Beck, M., Faist, J. and Gini, E. (2004) 'Broadband tuning of external cavity bound-to-continuum quantum-cascade lasers', *Appl. Phys. Lett.*, **84**, 1659–1661.

Maulini, R., Mohan, A., Giovannini, M., Faist, J. and Gini, E. (2006) 'External cavity quantum-cascade laser tunable from 8.2 to 10.4 μm using a gain element with a heterogeneous cascade', *Appl. Phys. Lett.*, **88**, 201113.

Maulini, R., Yarekha, D. A., Bulliard, J. M., Giovannini, M. and Faist, J. (2005) 'Continuous-wave operation of a broadly tunable thermoelectrically cooled external cavity quantum-cascade laser', *Opt. Lett.*, **30**, 2584–2586.

McCurdy, M. R., Bakhirkin, Y., Wysocki, G., Lewicki, R. and Tittel, F. K. (2007a) 'Recent advances of laser-spectroscopy-based techniques for applications in breath analysis', *J. Breath Res.*, **1**, 014001.

McManus, J. B., Kebabian, P. L. and Zahniser, W. S. (1995) 'Astigmatic mirror multipass absorption cells for long-path-length spectroscopy', *Appl. Opt.*, **34**, 3336–3348.

McCurdy, M. R., Bakhirkin, Y., Wysocki, G. and Tittel, F. K. (2007b) 'Performance of an exhaled nitric oxide and carbon dioxide sensor using quantum cascade laser-based integrated cavity output spectroscopy', *J. Biomed. Opt.*, **12**.

McManus, J. B., Kebabian, P. L. and Zahniser, W. S. (1995) 'Astigmatic mirror multipass absorption cells for long-path-length spectroscopy', *Appl. Opt.*, **34**, 3336–3348.

McManus, J. B., Nelson, D. D., Herndon, S. C., Shorter, J. H., Zahniser, M. S., Blaser, S., Hvozdara, L., Muller, A., Giovannini, M. and Faist, J. (2006) 'Comparison of cw and pulsed operation with a TE-cooled quantum cascade infrared laser for detection of nitric oxide at 1900 $cm^{-1}$', *Appl. Phys. B: Lasers and Optics*, **85**, 235–241.

McManus, J. B., Zahniser, M. S., Nelson, J. D. D., Shorter, J. H., Herndon, S., Wood, E. and Wehr, R. (2010) 'Application of quantum cascade lasers to high-precision atmospheric trace gas measurements', *Opt. Eng.*, **49**, 111124–11.

Mellqvist, J., Samuelsson, J., Rivera, C., Lefer, B. and M., P. (2007) 'Measurements of industrial emissions of VOCs, $NH_3$, $NO_2$ and $SO_2$ in Texas using the Solar Occultation Flux method and mobile DOAS', in *American Geophysical Union, Fall Meeting* Aug 20, 2007.

Meyer, J. R., Vurgaftman, I., Yang, R. Q. and Ram-Mohan, L. R. (1996) 'Type-II and type-I interband cascade lasers', *Electron. Lett.*, **32**, 45–46.

Miklos, A., Hess, P. and Bozoki, Z. (2001) 'Application of acoustic resonators in photoacoustic trace gas analysis and metrology', *Rev. Sci. Instrum.*, **72**, 1937–1955.

Miklos, A., Hess, P., Mohacsi, A., Sneider, J., Kamm, S. and Schafer, S. (1999) 'Improved photoacoustic detector for monitoring polar molecules such as ammonia with a 1.53 μm DFB diode laser', *AIP Conference Proceedings*, **463**, 126–128.

Moeskops, B. W. M., Cristescu, S. M. and Harren, F. J. M. (2006) 'Sub-part-per-billion monitoring of nitric oxide by use of wavelength modulation spectroscopy in combination with a thermoelectrically cooled, continuous-wave quantum cascade laser', *Opt. Lett.*, **31**, 823–825.

Mukherjee, A., Prasanna, M., Lane, M., Go, R., Dunayevskiy, I., Tsekoun, A. and Patel, C. K. N. (2008) 'Optically multiplexed multi-gas detection using quantum cascade laser photoacoustic spectroscopy', *Appl. Opt.*, **47**, 4884–4887.

Mürtz, M. and Hering, P. (2008) 'Online monitoring of exhaled breath using mid-infrared laser spectroscopy' in *Mid-Infrared Coherent Sources and Applications*, Springer Netherlands, 535–555.

Mürtz, P., Menzel, L., Bloch, W., Hess, A., Michel, O. and Urban, W. (1999) 'LMR spectroscopy: a new sensitive method for on-line recording of nitric oxide in breath', *J. Appl. Physiol.*, **86**, 1075–1080.

Ng, J., Kung, A. H., Miklós, A. and Hess, P. (2004) 'Sensitive wavelength-modulated photoacoustic spectroscopy with a pulsedoptical parametric oscillator', *Opt. Lett.*, **29**, 1206–1208.

O'Keefe, A. (1998) 'Integrated cavity output analysis of ultra-weak absorption', *Chem. Phys. Lett.*, **293**, 331–336.

O'Keefe, A. and Deacon, D. A. G. (1988) 'Cavity ring-down optical spectrometer for absorption measurements using pulsed laser sources', *Rev. Sci. Instrum.*, **59**, 2544–2551.

O'Keefe, A., Scherer, J. J. and Paul, J. B. (1999) 'cw Integrated cavity output spectroscopy', *Chem. Phys. Lett.*, **307**, 343–349.

Paldus, B. A., Harb, C. C., Spence, T. G., Zare, R. N., Gmachl, C., Capasso, F., Sivco, D. L., Baillargeon, J. N., Hutchinson, A. L. and Cho, A. Y. (2000) 'Cavity ring-down spectroscopy using mid-infrared quantum-cascade lasers', *Opt. Lett.*, **25**, 666–668.

Paldus, B. A. and Kachanov, A. A. (2005) 'An historical overview of cavity-enhanced methods', *Can. J. Phys.*, **83**, 975–999.

Paul, J. B., Lapson, L. and Anderson, J. G. (2001) 'Ultrasensitive absorption spectroscopy with a high-finesse optical cavity and off-axis alignment', *Appl. Opt.*, **40**, 4904–4910.

Petra, N., Zweck, J., Kosterev, A. A., Minkoff, S. E. and Thomazy, D. (2009) 'Theoretical analysis of a quartz-enhanced photoacoustic spectroscopy sensor', *Appl. Phys. B*, **94**, 673–680.

Pfeiffer, J., Kirsten, D., Kalkert, P. and Urban, W. (1981) 'Sensitive magnetic rotation spectroscopy of the OH free radical fundamental band with a colour centre laser', *Appl. Phys. B: Lasers and Optics*, **26**, 173–177.

Phillips, M. and Greenberg, J. (1991) 'Method for the collection and analysis of volatile compounds in the breath', *J. Chromatogr. B*, **564**, 242–249.

Phillips, M. C., Myers, T. L., Wojcik, M. D. and Cannon, B. D. (2007) 'External cavity quantum cascade laser for quartz tuning fork photoacoustic spectroscopy of broad absorption features', *Opt. Lett.*, **32**, 1177–1179.

Pushkarsky, M. B., Dunayevskiy, I. G., Prasanna, M., Tsekoun, A. G., Go, R. and Patel, C. K. N. (2006a) 'High-sensitivity detection of TNT', *Proc. Natl Acad. Sci. USA*, **103**, 19630–19634.

Pushkarsky, M. B., Tsekoun, A., Dunayevskiy, I. G., Go, R. and Patel, C. K. N. (2006b) 'Sub-parts-per-billion level detection of $NO_2$ using room-temperature quantum cascade lasers', *Proc. Natl Acad. Sci. USA*, **103**, 10846–10849.

Pushkarsky, M. B., Webber, M. E. and Patel, C. K. N. (2003) 'Ultra-sensitive ambient ammonia detection using $CO_2$-laser-based photoacoustic spectroscopy', *Appl. Phys. B*, **77**, 381–385.

Pushkarsky, M. B., Weida, M., Day T., Arnone, D., Pritchett, R., Caffey, D. and Crivello. S. (2008) 'High-power tunable external cavity quantum cascade laser in the 5–11 micron regime', *Anglais*, **6871**, 68711X.

Ramponi, A. J., Milanovich, F. P., Kan, T. and Deacon, D. (1988) 'High sensitivity atmospheric transmission measurements using a cavity ringdown technique', *Appl. Opt.*, **27**, 4606–4608.

Rao, G. N. and Karpf, A. (2011) 'Extremely sensitive detection of $NO_2$ employing off-axis integrated cavity output spectroscopy coupled with multiple line integrated absorption spectroscopy', *Appl. Opt.*, **50**, 1915–1924.

Rao, G. N. and Karpf, A. (2010) 'High sensitivity detection of $NO_2$ employing cavity ringdown spectroscopy and an external cavity continuously tunable quantum cascade laser', *Appl. Opt.*, **49**, 4906–4914.

Razeghi, M., Bai, Y., Slivken, S. and Darvish, S. R. (2010) 'High-performance InP-based midinfrared quantum cascade lasers at Northwestern University', *Opt. Eng.*, **49**, 111103.

Rey, J. M. and Sigrist, M. W. (2008) 'New differential mode excitation photoacoustic scheme for near-infrared water vapour sensing', *Sens. Actuators B*, **135**, 161–165.

Risby, T. and Tittel, F. K. (2010) 'Current status of mid-infrared quantum and interband cascade lasers for clinical breath analysis', *Opt. Eng.*, **49**, 000000–1.

Roller, C. B., Holland, B. P., McMillen, G., Step, D. L., Krehbiel, C. R., Namjou, K. and McCann, P. J. (2007) 'Measurement of exhaled nitric oxide in beef cattle using tunable diode laser absorption spectroscopy', *Appl. Opt.*, **46**, 1333–1342.

Rossi, A., Buffa, R., Scotoni, M., Bassi, D., Iannotta, S. and Boschetti, A. (2005) 'Optical enhancement of diode laser-photoacoustic trace gas detection by means of external Fabry-Perot cavity', *Appl. Phys. Lett.*, **87**, 041110.

Russell, M., Allen, D. T., Collins, D. R. and Fraser, M. P. (2004) 'Daily, seasonal, and spatial trends in PM2.5 mass and composition in Southeast Texas', *Aerosol Science and Technology*, **38**, 14–26.

Sabana, H., Fritsch, T., Boyomo Onana, M., Bouba, O., Hering, P. and Mürtz, M. (2009) 'Simultaneous detection of 14NO and 15NO using Faraday modulation spectroscopy', *Appl. Phys. B: Lasers and Optics*, **96**, 535–544.

Sayres, D. S., Moyer, E. J., Hanisco, T. F., Clair, J. M., Keutsch, F. N., O'Brien, A., Allen, N. T., Lapson, L., Demusz, J. N., Rivero, M., Martin, T., Greenberg, M., Tuozzolo, C., Engel, G. S., Kroll, J. H., Paul, J. B. and Anderson, J. G. (2009) 'A new cavity based absorption instrument for detection of water isotopologues in the upper troposphere and lower stratosphere', *Rev. Sci. Instrum.*, **80**, 44102–44102.

Scherer, D. R., Montoya, J., Hensley, J. M. and Allen, M. G. (2009) *Tunable External-Cavity Quantum Cascade Laser Sources for Gas Sensing and Spectroscopy,* translated by Optical Society of America, JTuD18.

Scherer, J. J., Paul, J. B., O'Keefe, A. and Saykally, R. J. (1997) 'Cavity ringdown laser absorption spectroscopy: History, development, and application to pulsed molecular beams', *Chem. Rev.*, **97**, 25–51.

Schilt, S. and Thévenaz, L. (2006) 'Wavelength modulation photoacoustic spectroscopy: Theoretical description and experimental results', *Infrared Phys. Techn.*, **48**, 154–162.

Schilt, S., Thévenaz, L. and Robert, P. (2003) 'Wavelength modulation spectroscopy: combined frequency and intensity laser modulation', *Appl. Opt.*, **42**, 6728–6738.

Seinfeld, J. and Pandis, S. (1998) *Atmospheric Chemistry and Physics: From Air Pollution to Climate Change*, Wiley, New York.

Shorter, J. H., Nelson, D. D., McManus, J. B., Zahniser, M. S. and Milton, D. K. (2010) 'Multicomponent breath analysis with infrared absorption using room-temperature quantum cascade lasers', *Sensors Journal, IEEE*, **10**, 76–84.

Sigrist, M. W. and Thoeny, A. (1993) *Atmospheric trace gas monitoring by $CO_2$ laser photoacoustic spectroscopy,* translated by Harold, I. S. and Ulrich, P., SPIE, 174–184.

Smith, D. and Španěl, P. (2005) 'Selected ion flow tube mass spectrometry (SIFT-MS) for on-line trace gas analysis', *Mass Spectrom. Rev.*, **24**, 661–700.

Smith, J. M., Bloch, J. C., Field, R. W. and Steinfeld, J. I. (1995) 'Trace detection of $NO_2$ by frequency-modulation-enhanced magnetic rotation spectroscopy', *J. Opt. Soc. Am. B*, **12**, 964–969.

So, S., Amiri Sani, A., Zhong, L. and Tittel, F. (2009) 'Laser spectroscopic trace-gas sensor networks for atmospheric monitoring applications', in *ESSA Workshop '09*, San Francisco, California, USA.

So, S., Jeng, E., Smith, C., Krueger D. and Wysocki, G. (2010) Next generation infrared sensor instrumentation: remote sensing and sensor networks using the openPHOTONS repository, translated by Marija, S. and Gonzalo, P., SPIE, 780818.

So, S., Jeng, E. and Wysocki, G. (2011) 'VCSEL based Faraday rotation spectroscopy with a modulated and static magnetic field for trace molecular oxygen detection', *Appl. Phys. B*, **102**, 279–291.

Sonnenfroh, D. M., Rawlins, W. T., Allen, M. G., Gmachl, C., Capasso, F., Hutchinson, A. L., Sivco, D. L., Baillargeon, J. N. and Cho, A. Y. (2001) 'Application of balanced detection to absorption measurements of trace gases with room-temperature, quasi-cw quantum-cascade lasers', *Appl. Opt.*, **40**, 812–820.

Spagnolo, V., Kosterev, A., Dong, L., Lewicki, R. and Tittel, F. (2010) 'NO trace gas sensor based on quartz-enhanced photoacoustic spectroscopy and external cavity quantum cascade laser', *Appl. Phys. B: Lasers and Optics*, **100**, 125–130.

Sukhorukov, O., Lytkine, A., Manne, J., Tulip, J. and Jager, W. (2006) *Cavity ring-down spectroscopy with a pulsed distributed feedback quantum cascade laser,* translated by Manijeh, R. and Gail, J. B., SPIE, 61270A.

Thorpe, M. J., Balslev-Clausen, D., Kirchner, M. S. and Ye, J. (2008) 'Cavity-enhanced optical frequency combspectroscopy: application to human breathanalysis', *Opt. Express*, **16**, 2387–2397.

Tittel, F. K., Kosterev, A. A., Bakhirkin, Y. A., Roller, C. B., Weidmann, D. and Curl, R. F. (2003) *Chemical sensors based on quantum cascade lasers*, translated by 893–894 Vol.2.

Troccoli, M., Wang, X. and Fan, J. (2010) 'Quantum cascade lasers: high-power emission and single-mode operation in the long-wave infrared ($\lambda > 6$ μm)', *Opt. Eng.*, **49**, 111106–9.

Tsai, T. and Wysocki, G. (2010) 'External-cavity quantum cascade lasers with fast wavelength scanning', *Appl. Phys. B: Lasers and Optics*, **100**, 243–251.

Vurgaftman, I., Kim, M., Kim, C. S., Bewley, W. W., Canedy, C. L., Lindle, J. R., Abell, J. and Meyer, J. R. (2010) *Challenges for mid-IR interband cascade lasers*, 1 ed., translated by Belyanin, A. A. and Smowton, P. M., San Francisco, California, USA: SPIE, 761619-10.

Webber, M. E., Pushkarsky, M. and Patel, C. K. N. (2003) 'Fiber-amplifier-enhanced photoacoustic spectroscopy with near-infrared tunable diode lasers', *Appl. Opt.*, **42**, 2119–2126.

Weida, M. J., Caffey, D., Rowlette, J. A., Arnone, D. F. and Day, T. (2010) 'Utilizing broad gain bandwidth in quantum cascade devices', *Opt. Eng.*, **49**, 111120–5.

Weidmann, D., Wysocki, G., Oppenheimer, C. and Tittel, F. K. (2005) 'Development of a compact quantum cascade laser spectrometer for field measurements of $CO_2$ isotopes', *Appl. Phys. B: Lasers and Optics*, **80**, 255–260.

Werle, P. (2011) 'Accuracy and precision of laser spectrometers for trace gas sensing in the presence of optical fringes and atmospheric turbulence', *Appl. Phys. B: Lasers and Opt.*, **102**, 313–329.

Werle, P., Mücke, R. and Slemr, F. (1993) 'The limits of signal averaging in atmospheric trace-gas monitoring by tunable diode-laser absorption spectroscopy (TDLAS)', *Appl. Phys. B: Lasers and Opt.*, **57**, 131–139.

Westhoff, M., Litterst, P., Freitag, L., Urfer, W., Bader, S. and Baumbach, J.-I. (2009) 'Ion mobility spectrometry for the detection of volatile organic compounds in exhaled breath of patients with lung cancer: results of a pilot study', *Thorax*, **64**, 744–748.

Willer, U. and Schade, W. (2009) 'Photonic sensor devices for explosive detection', *Anal. Bioanal. Chem.*, **395**, 275–282.

Wittmann, A., Bonetti, Y., Fischer, M., Faist, J., Blaser, S. and Gini, E. (2009) 'Distributed-Feedback Quantum-Cascade Lasers at 9 μm Operating in Continuous Wave Up to 423 K', *Photon. Technol. Lett., IEEE*, **21**, 814–816.

Wittmann, A., Hugi, A., Gini, E., Hoyler, N. and Faist, J. (2008) 'Heterogeneous high-performance quantum-cascade laser sources for broad-band tuning', *IEEE J. Quantum Electron.*, **44**, 1083–1088.

Wojcik, M. D., Phillips, M. C., Cannon, B. D. and Taubman, M. S. (2006) 'Gas-phase photoacoustic sensor at 8.41 μm using quartz tuning forks and amplitude-modulated quantum cascade lasers', *Appl. Phys. B*, **85**, 307–313.

Wysocki, G., Curl, R. F., Tittel, F. K., Maulini, R., Bulliard, J. M. and Faist, J. (2005) 'Widely tunable mode-hop free external cavity quantum cascade laser for high resolution spectroscopic applications', *Appl. Phys. B*, **81**, 769–777.

Wysocki, G., Kosterev, A. A. and Tittel, F. K. (2006) 'Influence of molecular relaxation dynamics on quartz-enhanced photoacoustic detection of CO2 at $\lambda$ =2 μm', *Appl. Phys. B: Lasers and Optics*, **85**, 301–306.

Wysocki, G., Lewicki, R., Curl, R. F., Tittel, F. K., Diehl, L., Capasso, F., Troccoli, M., Hofler, G., Bour, D., Corzine, S., Maulini, R., Giovannini, M. and Faist, J. (2008) 'Widely tunable mode-hop free external cavity quantum cascade lasers for high resolution spectroscopy and chemical sensing', *Appl. Phys. B*, **92**, 305–311.

Xu, G., Li, A., Li, Y., Wei, L., Zhang, Y., Lin, C. and Li, H. (2006) 'Low threshold current density distributed feedback quantum cascade lasers with deep top gratings', *Appl. Phys. Lett.*, **89**, 161102.

Yang, R. Q. (1995) 'Infrared laser based on intersubband transitions in quantum wells', *Superlattices and Microstruct.*, **17**, 77–83.

Yao, Y., Charles, W. O., Tsai, T., Chen, J., Wysocki, G. and Gmachl, C. F. (2010a) 'Broadband quantum cascade laser gain medium based on a "continuum-to-bound" active region design', *Appl. Phys. Lett.*, **96**, 211106.

Yao, Y., Wang, X., Fan, J.-Y. and Gmachl, C. F. (2010b) 'High performance "continuum-to-continuum" quantum cascade lasers with a broad gain bandwidth of over 400 cm-1', *Appl. Phys. Lett.*, **97**, 081115.

Ye, J., Ma, L.-S. and Hall, J. L. (1998) 'Ultrasensitive detections in atomic and molecular physics: demonstration in molecular overtone spectroscopy', *J. Opt. Soc. Am. B*, **15**, 6–15.

Yu, J. S., Slivken, S., Darvish, S. R., Evans, A., Gokden, B. and Razeghi, M. (2005) 'High-power, room-temperature, and continuous-wave operation of distributed-feedback quantum-cascade lasers at lambda ~ 4.8 mm', *Appl. Phys. Lett.*, **87**, 041104.

Zahniser, M. S., Nelson, D. D., McManus, J. B., Kebabian, P. L. and Lloyd, D. (1995) 'Measurement of trace gas fluxes using tunable diode laser spectroscopy', *Phil. Trans.: Physical Sci. Eng.*, **351**, 371–382.

Zaugg, C. A., Lewicki, R., Day, T., Curl, R. F. and Tittel, F. K. (2011) 'Faraday rotation spectroscopy of nitrogen dioxide based on a widely tunable external cavity quantum cascade laser.', *Proc. of SPIE 7945: 50O-1*.

Zhao, W., Wysocki, G., Chen, W., Fertein, E., Le Coq, D., Petitprez, D. and Zhang, W. (2011) 'Sensitive and selective detection of OH radicals using Faraday rotation spectroscopy at 2.8 μm', *Opt. Express*, **19**, 2493–2501.